COMPUTATIONAL ANALYSIS OF FLOW CHARACTERISTICS AROUND HYBRID SPUR DYKES

A Dissertation submitted in partial fulfillment of the requirement for the Award of degree of

MASTER OF TECHNOLOGY

IN

HYDRAULICS & FLOOD ENGINEERING

BY

SUNIL KUMAR
(ROLL NO. 2K14/HFE/17)

Under the Guidance of

Dr. RAKESH KUMAR

Professor
Department of Civil Engineering
Delhi Technological University
Delhi

DELHI TECHNOLOGICAL UNIVERSITY
(FORMERLY DELHI COLLEGE OF ENGINEERING)
DELHI - 110042
July-2016

CANDIDATE'S DECLARATION

I do hereby certify that the work presented is the report entitled "**computational analysis of flow characteristics around hybrid spur dykes**" in the partial fulfillment of the requirements for the award of the degree of "Master of Technology" in Hydraulics & Flood engineering submitted in the Department of Civil Engineering, Delhi Technological University, is an authentic record of my own work carried out from January 2016 to July 2016 under the supervision of Dr. Rakesh Kumar (Professor), Department of Civil Engineering.

I have not submitted the matter embodied in the report for the award of any other degree or diploma.

Sunil Kumar

Date: /7/16 (2K14/HFE/17)

CERTIFICATE

This is to certify that above statement made by the candidate is correct to best of my knowledge.

Dr. Rakesh Kumar
(Professor)
Department of Civil Engineering
Delhi Technological University

ACKNOWLEDGEMENT

I take this opportunity to express my profound gratitude and deep regards to Dr. Rakesh Kumar (Professor, Civil Engineering Department, DTU) for his exemplary guidance, monitoring and constant encouragement throughout the course of this project work. The blessing, help and guidance given by him from time to time shall carry me a long way in life on which I am going to embark.

I would also like to thank Dr. Nirendra Dev (Head of Department, Civil Engineering Department, DTU) for extending his support and guidance.

Professors and faculties of the Department of Civil Engineering, DTU, have always extended their full co-operation and help. They have been kind enough to give their opinions on the project matter; I am deeply obliged to them. They have been a source of encouragement and have continuously been supporting me with their knowledge base, during the study. Several of well-wishers extended their help to me directly or indirectly and we are grateful to all of them without whom it would have been impossible for me to carry on my work.

ABSTRACT

Spur dykes are river training structures commonly installed for erosion control and bank protection purpose. The installation of groyne however results in highly turbulent flow resulting in high local scour in the vicinity of the tip of groyne. Several research works have shown that impermeable groynes are more effective in river training but results in high local scour, permeable groynes results in lower local scouring but are not effective as river training structure. In this dissertation work an attempt is made to combine impermeable and permeable groynes and analyze the performance of resulting hybrid groynes as an alternative groyne with minimization of local scouring phenomenon. In general, the flow structure around a hybrid spur dyke has the combined effect of a permeable and an impermeable spur dykes. Flow around the hybrid groyne is analyzed by numerical modelling using CFD code ANSYS FLUENT. The Realizable K-e model is used for turbulence modelling. The groynes are tested for their performance at various flow depth and Froude number. Performance of these hybrid spurs is compared with impermeable and permeable spur based on the tip velocity, maximum velocity, and separation length. The bandall structure with permeable base is found to provide separation length comparable to impermeable groynes and at the same time shows considerable reduction in velocity and bed shear amplification.

CONTENTS

LIST OF FIGURES

LIST OF TABLES

LIST OF SYMBOLS

Symbol	Title
V_{app}	Velocity of approach to spur in m/s
V_{tip}	Tip velocity at spur in m/s
$V_{tip(exp)}$	Tip velocity obtained experimentally in m/s
$V_{tip(num)}$	Tip velocity obtained numerically in m/s
V_{max}	Maximum velocity near spur in m/s
X	distance across the direction of flow from the tip of the spur in m
Z	distance along the direction of flow from the tip of spur in m
τ_m	Maximum bed shear stress in pascals
τ_0	Shear stress of undisturbed approach flow in pascals
τ_m/τ_0	Shear stress amplification
l	Length of spur in m
L	Separation length in m
F	Froude number
Y	Flow depth

CHAPTER 1 INTRODUCTION

Spur dykes are elongated hydraulic structures protruding from the bank of the river perpendicularly or at some angle towards centre of stream. These structures are widely used for river training work in alluvial rivers for a number of different Purposes such as bank protection, maintenance of navigation channel, improving river ecology etc. they protect the bank from which they are extending by deflecting the flow away from the bank, the water is unable to take a sharp embayment and the bank gets protected for some distance upstream or downstream. By constructing series of spur dikes perpendicularly to the river banks the flow is kept away from the erodible banks. At the same time the laterally confined flow attains a sufficiently high velocity to keep the navigation channel at proper depth. They are made of gravel, stone, earth embankment, rock, or piles, beginning at the riverbank with a root and ending at the regulation line with a head.

An interesting criteria in the design of these structures is the disturbance the structure will cause in the flow field, Local erosion and siltation induced etc. the study of flow field hence becomes necessary to find how far downstream the disturbances extend. High strength vortices forms near the tip of groyne. The tip of the groyne is hence subjected to tremendous forces.

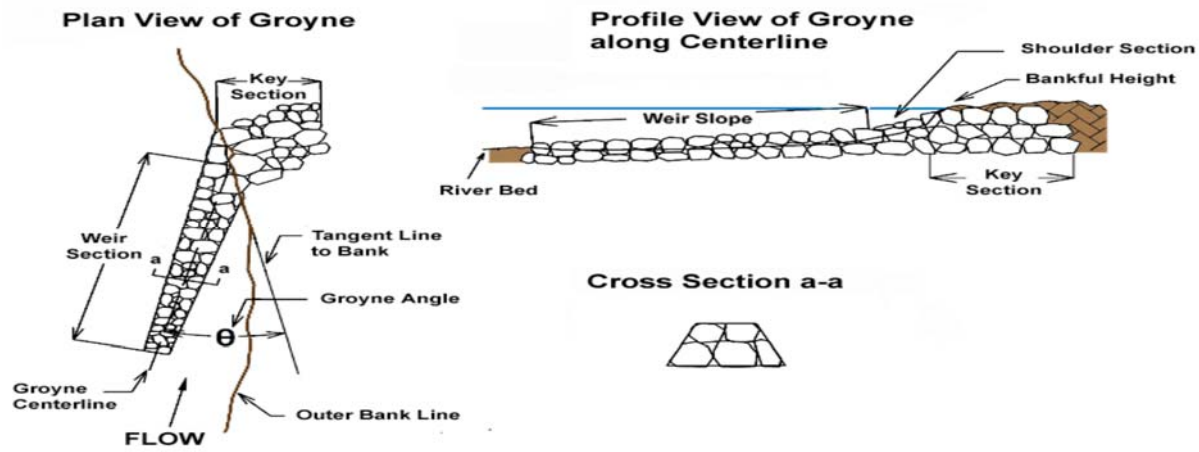

Fig 1.1 cross sectional view of typical groyne

Groynes can be classified as normal, reflecting and attracting which depend on their alignment. A groyne built perpendicularly to the flow is termed as normal or ordinary groyne. A groyne pointing upstream has the property of repelling the flow away from it and is known as repelling groyne, whereas groyne pointing downstream have a tendency to attract the flow towards it and is called as attracting groyne.

Groynes can also be classified as impermeable and permeable groyne.

Impermeable groyne:

Impermeable groynes also termed as embankment groyne or solid groyne may be rock fill embankment or earthen embankment armoured with stone pitching etc. these groynes do not permit any significant flow through them.

Permeable groyne:

These groynes permit restricted flow through them. These are usually tree spurs or balli spurs driven in the bed.

A lot of research works have been done on impermeable groynes and groynes of varying permeability. However works on combination of the two is very scarce. Such combinations can be termed as hybrid groynes, and are explained as follows.

Hybrid groyne:

These are the different combinations of impermeable and permeable groyne arrangements. Various combinations can be made some of them are as under.

- Impermeable root near bank and permeable at head.
- Permeable near bank and impermeable towards head.
- Permeable lower portion and impermeable upper portion. This structure with permeable lower portion is commonly known as Bandall type structure.

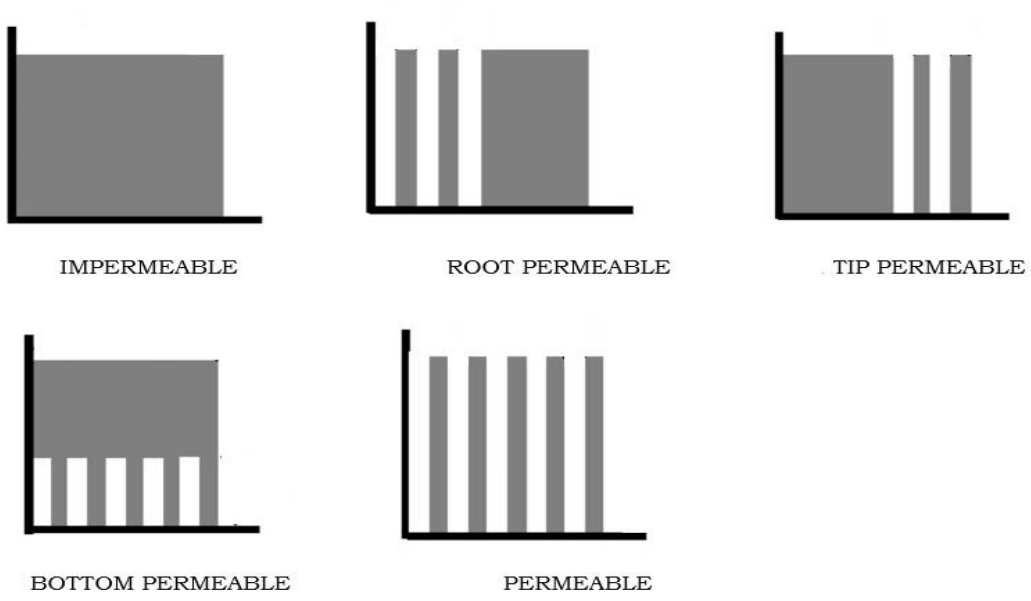

Fig 1.2 Some typical hybrid groynes

1.1 Flow around a spur dyke

When a groyne is installed in a river it causes sudden reduction in the width of the stream. The width reduction causes increase in velocities and flow separation occurs as shown in the fig3. Recirculation zone is formed downstream due to the difference in velocities in main flow and recirculation zone flow, shear layer is formed between main flow zone and recirculation zone. A large vortex is formed in the recirculation zone coupled with some small vortices. Further downstream the recirculation zone reduces and finally mixes with main flow to return to the main channel flow pattern. This distance after which recirculation zone mixes with main flow is called as separation length.

Impermeable groynes are relatively active structures and permeable spur dykes are relatively passive ones regarding their controls on the flow. Impermeable spur dykes have great impacts on the local flow structures. The flow velocity is altered in both its direction and its magnitude, resulting in significant toe scouring and corresponding wake deposition.

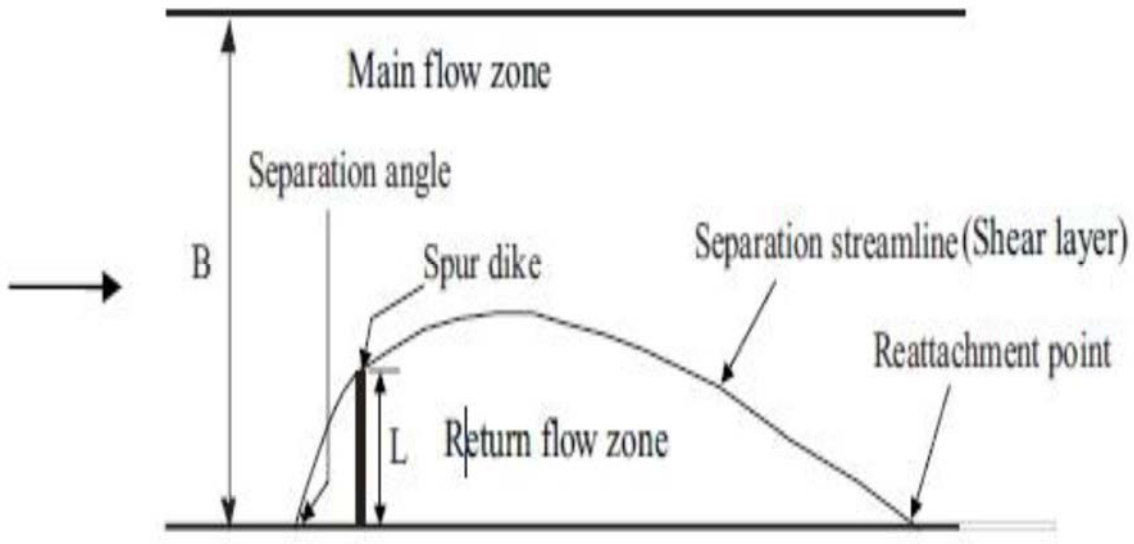

Fig 1.3 Flow around a single groyne

1.2 Objective of Dissertation

i. To investigate the effect of groyne installation on flow field.

ii. To investigate the performance of different combinations of permeable and impermeable structures as groyne (hybrid groyne) and hence identify the best combination for spur dyke based on the results of separation length and maximum bed shear stress.

iii. To identify the maximum velocity in the area near the spur and its position from the tip of the spur.

iv. To study the streamlines and vortex for different hybrid groyne structures.

1.3 Scope of the project

Construction of a spur dike perpendicular to river flow decreases the width of river and causes flow separation around the spur dike and recirculation zone is created downstream. Due to contraction of streamlines and increasing velocity, the river bed is subjected to extensive scouring. Local scour around spur dikes is a

problem because of the potential for high and damaging erosion which may even cause structural failures creating hazards to the public.

In most of the cases impermeable and permeable groynes are used presently however impermeable groynes have demerit of high local scouring near the tip which can also be dangerous for groyne structure. Whereas in case of permeable groyne the diversion of flow is much small and comparatively more number of groynes will be required for same diversion in flow field. Hence flow around different hybrid structures is analysed in this project work to see their applicability as groyne.

The study of shear amplification factor and maximum bed shear will provide us location of potential scour zones and hence will help in choosing the best suitable combination to be used as groyne. Tip velocity and maximum velocity values will provide for predicting scour factors. The study of separation length will assist in determining the installation interval of successive groynes.

ANSYS FLUENT v.15 has been used throughout this dissertation work for the analysis of flow field around groynes. This CFD package has may closure models for turbulence modelling. In this project work realizable k-e model is used with enhanced wall function for wall water interaction.

1.4 Introduction to ANSYS FLUENT

Computational fluid dynamics is a mathematical tool used for modelling fluid dynamics problems using computers. Due to its many advantages over physical models it has emerged a lot of interest. The basic principle in the application of CFD is to determine fluid flow in-detail by solving a system of non-linear governing equations over the region of interest, after applying specified boundary conditions. The CFD based simulation confides on combined numerical accuracy, modelling precision and computational cost.

FLUENT is 3D CFD software package which can be used for numerical simulation of nearly all kind of fluid problems. It uses finite volume approach to solve 3D incompressible continuity and Reynolds-averaged Navior-Stokes equations. Fluent offers a large number of turbulence models such as k -ε, RNG k -ε, Reynolds stress model, Spalart-Allmaras model, shear stress transport k-Ω model, large eddy simulation, detached eddy simulation models etc. The pressure velocity coupling can be done using SIMPLE, SIMPLEC or PISO algorithms. ANSYS Fluent is integrated into the unified ANSYS workbench platform. ANSYS Fluent software gives complete mesh adaptability, including the ability to solve flow problems using unstructured meshes that can be produced about complex geometries. It supports quadrilateral, triangular, tetrahedral, hexahedral, pyramid, prism and polyhedral type of meshes. It also allows dynamic refinement or coarsening of the mesh based on condition. ANSYS Fluent runs conveniently for all physical models and flow types including steady-state or transient, incompressible or compressible flows, laminar or turbulent flows and Newtonian or non-Newtonian flows. Post-processing tools for ANSYS Fluent can be used to make animations, graphics and reports that make it easy to show results. Path lines, vector plots, contour can also be plotted in CFX post embedded in the ANSYS Workbench.

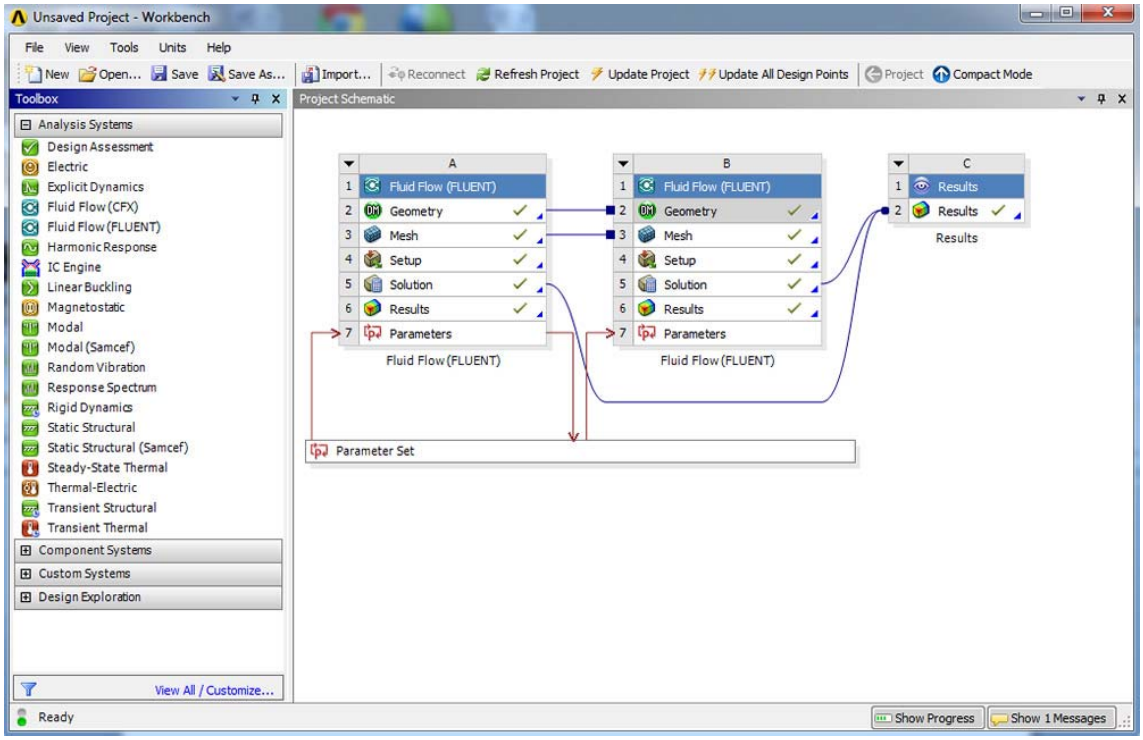

Fig 1.4 Overview of ANSYS FLUENT

1.5 Organisation of the dissertation work:

The work presented in this report has been organised into six chapters. The first chapter gives a brief introduction about flow characteristics around groyne, states the importance of the matter and aim of the study. Chapter two gives the review of previous research works on the topic. The methodology involved is presented in chapter 3. The numerical model data output from ANSYS fluent is given in chapter 4. The results and discussions are enlisted in chapter 5 and chapter 6 concludes the study with future scope of study.

CHAPTER 2-LITERATURE REVIEW

Flow around spurs have been an interesting phenomenon for researchers in the past and many research work have been done for analysing flow around groynes. The first research in this respect was carried out by Francis et al [1]. They conducted various experimental study to examine downstream groyne separation zone in a rectangular flume, but they did not measure velocities. They found out that the extent of the eddy zone on the channel bed is strongly influenced by lateral slope of groyne. Also they found out that the length of eddy zone does not show any clear dependence on width contraction ratio and lateral slope.

Rajaratnam and Nwachukwu [2], performed experimental study on groynes installed on smooth and uniform roughness bed for the analysis of structure of turbulent flow around groynes and studied bed shear stress near tip.

Asayama and Kadota [3] conducted field investigation to measure the sizes of groynes as well as bed morphology around the groynes. A Particle tracking velocimetry (PTV), 3D flow numerical analysis of flow and bed variation around the groynes were investigated. They proposed a simple arrangement of river structure for stable bed morphology.

Tingsanchali and Maheswaran [4], computed depth-averaged velocity and bottom shear stress distributions in a rectangular channel near groyne using 2-D depth averaged model. They found that the bottom shear stress is found to be largely influenced by the 3-D effects and introduced a 3-D correction factor to improve the computed bottom shear stresses.

Ouillon and Dartus [5], used the porosity method to track the free surface for flow computations around spur dyke. They concluded that maximum shear stress is located at the upstream corner of the tip of the spur.

Mioduszewski et al [6], performed experimental study on effect of permeability on flow characteristics and reported lesser erosion in permeable spurs.

Ettema and Muste [7], performed a series of flume experiments to determine the scale effects in small scale models of flow around a single spur dike placed in a fixed and flat bed channel. They used hydraulic similitude based on the shear stress parameter u^*0 / u^*C.

Baba et al [8] performed experimental study on permeability of groyne to illustrate the difference of the flow pattern around the foot of the spur dyke between impermeable and permeable spurs.

Uijttewaal [9], performed experiments in physical model of a river reach geometrically scaled to 1:40. Four different types of groynes were tested and all of them were arranged in an array of five identical groyne fields. Flow velocities were measured using PTV. The design of experiment was such that the cross sectional area blocked by the groyne was same in all the experiments. They concluded that turbulence properties near and downstream of the groyne can be manipulated by changing the permeability and slope of the groyne head.

Yeo et al [10]. performed experimental study in a flat and fixed open channel with groynes of different permeabilities, relative lengths and approach velocities. He suggested an empirical equation for tip velocity in terms of approach velocity and groyne area ratio. He also suggested an empirical equation describing the relationship between the ratio of the separation length to groyne length and Froude number.

Kang et al. [11] performed hydraulic experiments in fixed and movable beds to examine the flow pattern, bed change and scour depth and hole around a groyne. Both permeable and impermeable groynes were used for testing. The maximum scour depth for each groyne type moved along a linearly downward path with increasing permeability. The scour depth was decreasing with increase in permeability. The maximum scour

depth was greatest with perpendicular groyne. The scour area was much larger for impermeable groyne than permeable groyne.

Ghani et al. [12] performed numerical study on flow around groynes and studied streamlines over vertical sections and turbulence kinetic energy. He found that TKE is affected considerably due to presence of spur-dike and was found maximum behind the spur dike and distributed over the major part of the cross section for some distance behind the dike.

Ghaldarbandi [13] et al. performed numerical study on lateral slope of impermeable groynes on varying cross shore bed slope. They used standard K-e model for numerical modelling.

Zhang et al. [14] performed experimental study on the local flow and bed variation around different types of spur dykes in sediment mixtures to study the scour patterns for different structures. He used 3 different type of hybrid structures along with impermeable and permeable structure. He concluded that desirable flow characterstics can be achieved by hybrid permeability groyne. He also found that the max scour depth is considerably less for bandall like structure.

Yossef and Vriend [15] performed experiments on a fixed bed flume for a schematized river reach with groynes on one side to study the dynamics of the flow near groynes. The flume was made to a geometrical scale of 1:40 based on the dimensions of the river waal. Large scale velocity fluctuations were found in all the test cases. The submerged groynes showed different turbulence pattern from the emerged groynes. The sediment transport rate was found to be proportional to the velocity to a certain power.

Xuelin et al. [16] used large eddy simulations to model the three dimensional flows around a non-submerged spur dike. The finite volume method was used to discretize the Navier-Stokes equations, and the SIMPLEC algorithm was used to solve them. The computational results were in good agreement with experimental results.

McCoy et al. [17] performed a Large eddy simulation(LES) on the groyne field in a straight open channel. The mean velocity at the free surface was found to be in good agreement with the experimental results. The bed shear stress was found to be more in the region close to downstream of the groyne.

Safarzadeh et al. [18] performed experimental measurements to investigate the head shape effects on bed shear stress distribution around single straight and T-shape groynes. Distribution of shear stress was more uniform downstream of the T-shape groyne.

Yazdi et al. [19] used Fluent software to study the flow patterns around a single spur dike. He used standard k-ω turbulence model with VOF method to get the results. By comparing the reults with experimental data, the model was found to produce flow around a spur dike with sufficient accuracy.

Shahrokhi and Sarveram [20] used Flow-3D software to provide a numerical model of groyne surrounding flow by using large eddy turbulence model while studying the effects of these factors on separation length and width of separation region behind a groyne by applying various installation angles, groyne lengths and flow velocities. The separation region length and width were maximum for angle of installation of 105^0.

Hakimzadeh et al. [21] studied the effect of structural slope of model groynes on scour reduction. Total 8 tests were performed with different lateral slopes of groynes. The experimental results showed that the maximum scour depth at the head of groynes was reduced by 22% by reducing the structural slopes of groynes. The transported sediments volume for mildest lateral slope groyne reduced significantly when compared with rectangular groyne.

Mansoori et al. [22] investigated three-dimensional flow structure around two simple series of groynes with different shapes of head using a numerical model known as SSIIM. Two case studies were considered: a simple series of straight groynes and a simple series of groynes with T-shape head. A brief discussion about

the physics of flow was done in order to compare the performance of a series of T-shape groynes with that of straight ones based on the primary objectives of the designs of the groynes.

Acharya et al. [23] presented a 3D numerical simulation of turbulent flow field around a series of three experimental dikes in a flat and scoured bed surface using Flow-3d software. They used three different numerical models in Flow-3d to compare the results from the experimental data.

Ghaidarbandi et al. [24] studied the effects of the cross shore and groyne wall slopes on flow parameters around an impermeable groyne using Fluent software. They used k-ϵ RNG model to analyse the flow. The numerical model results were in good agreement with the experimental work and they revealed that by increasing the cross shore bed slope magnitude of maximum velocity and bed shear stress decreased. These valued decreased further as the structural slope was reduced.

Shamloo and Pirzadeh [25] used Fluent software to validate the experimental results of Yeo et al. [10]. They used Reynolds stress turbulence model(RSM) in Fluent software to estimate the turbulent flow field. The numerical results showed satisfying agreement with the experimental data.

Karami et al. [26] investigated scour phenomenon around a series of impermeable, non-submerged spur dikes with both experimental and numerical methods. The experiments were conducted with different states of flow intensity. For numerical simulation SSIIM 2.0 was used to compute the data. They used RNG k-ϵ turbulence model and compared experimental and numerical data.

In this dissertation work the experimental setup and hybrid spur dykes used by Zhang et al. [14] is modelled numerically using ANSYS FLUENT software.

Chapter 3: METHODOLOGY

3.1 Overview of the study:

In this study, impermeable and permeable spur dykes are combined in different ways and the hydraulic and morphological consequences of the resulted new types of spur dykes in flat bed is analysed. Five types of spur dykes are analysed in this study, as shown in Fig.3.1. the permeable pat of all the structures is kept 50% permeable.

1. Impermeable spur (S1)
2. root part permeable and the tip part impermeable (S2)
3. Root part impermeable and tip part permeable (S3)
4. upper part impermeable and the lower part permeable (S4)
5. permeable spur (S5).

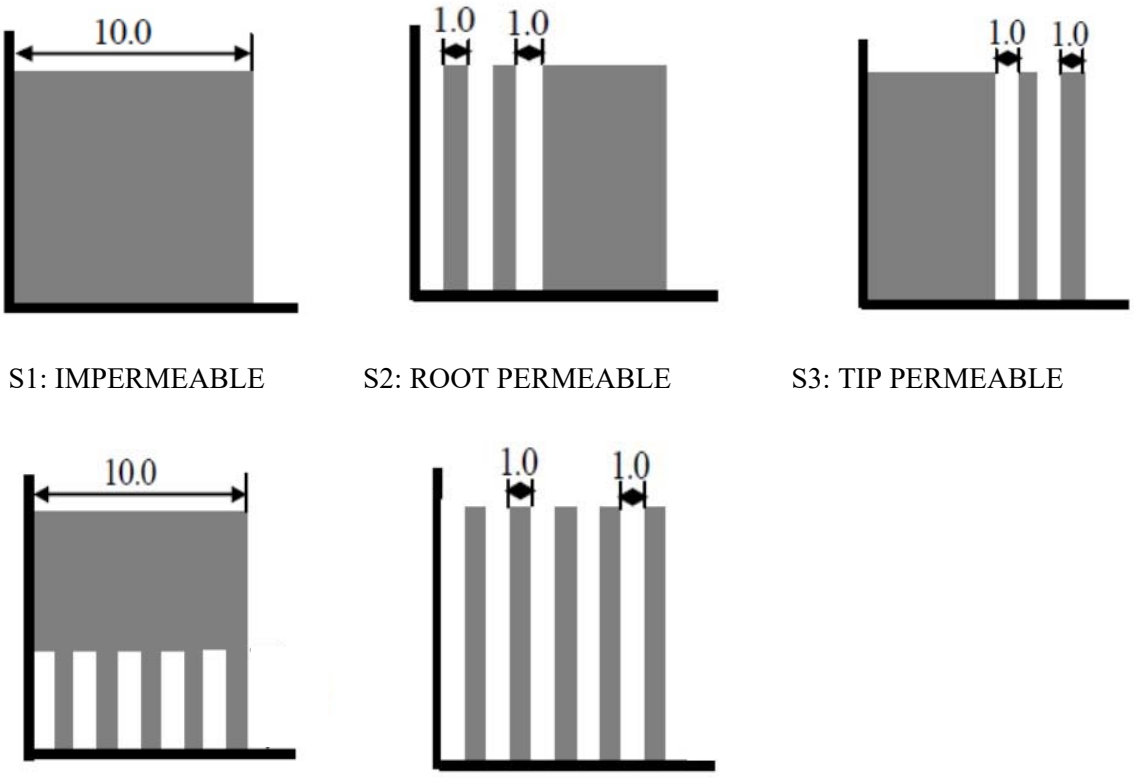

S1: IMPERMEABLE S2: ROOT PERMEABLE S3: TIP PERMEABLE

S4: BOTTOM PERMEABLE (Bandall Structure) S5: 50% PERMEABLE

FIG. 3.1 Spur dykes used in the study; permeable part is 50% permeable; all dimensions are in cm

The experimental setup performed by Zhang et al. is remodelled using fixed flatbed on ANSYS FLUENT for this study. The experimental setup consisted of a flume which is 8m long, 40cm wide and 40cm in deep. The length of spur is kept at 10cm and permeability is provided by using 1cm diameter cylinders alternatively. The

permeability of permeable regions of spurs is 50%. The spur dyke is installed perpendicular to the flume wall and remains non-submerged throughout the experiments.

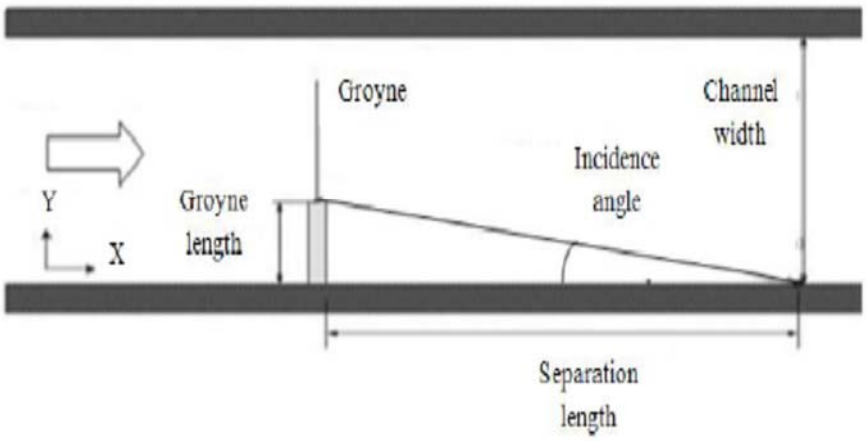

Fig.3.2 Schematic sketch of the experimental setup

The flow around these spurs is analysed at three different flow depths, for four different Froude numbers. Hence a total of sixty models are analysed.

3.2 Nomenclature of the models

F1	0.25
F2	0.4
F3	0.5
F4	0.75

Y1	3.75 cm
Y2	5.00 cm
Y3	6.25 cm

Impermeable spur	S1
Root part permeable and the tip part impermeable	S2
Root part impermeable and tip part permeable	S3
Upper part impermeable and the lower part permeable	S4
Permeable spur	S5

3.3 Numerical method

A CFD code, namely ANSYS FLUENT, has been used in the present work for analysis of flow around groyne. The finite volume numerical approach is used for the solution of conservation equations. Numerical modelling involves solution of the Navier–Stokes equations, which are based on the assumptions of conservation of mass and momentum within a moving fluid. The flow around a spur dyke is highly turbulent and Realizable k-e turbulence closure model is used for turbulence modelling. The near wall interactions are simulated using enhanced wall treatment function.

The process of the numerical simulation involves three steps:

(a) Pre-Processing

- Geometry set-up and domain discretization.
- Defining the flow conditions (models for computation) and boundary conditions.

(b) Solver

- The equation emphasizes over and over till desirable level of accuracy is attained.

(c) Post processing

- Analysis of result.

3.3.1 Model validation

Before the hybrid groynes are analysed the numerical model is validated for its performance in analysis of flow around groyne. The validation of model is done by modelling the experimental work of yeo.et al. and comparing the numerical result with the experimental results obtained by yeo.et.al.

The experimental setup of Yeo et al. consisted of flume 40 m long, 2.0 m wide and 0.65 m deep. The spur model used was made of acrylic and permeability is provided in case of permeable groynes by changing the interval of cylinders of 2cm diameter. The experiments on spur length 0.2m, 0.3 and 0.4m for 0%, 20%, and 40% permeability are modelled for the purpose of model validation.

Symbol	length
L1	0.2m
L2	0.3m
L3	0.4m

Symbol	Permeability
P1	0%
P2	20%
P3	40%

3.3.2 Geometry setup

ANSYS FLUENT has its own geometry modelling embedded in the workbench and is used for modelling the geometry. Geometry for three different flow depth are created for all structures considered. A total of fifteen different geometries are made.

The width of the flume is taken as 40 cm and length of the spurs is taken as 10 cm. The flume is kept symmetrical about x axis and the groyne is kept at the location of Z=0 in xz plane. And flow occurs perpendicular to xy plane in negative Z direction ie. Negative Z coordinate represent downstream of the groynes. The created geometries for all cases is shown in fig.3.3.

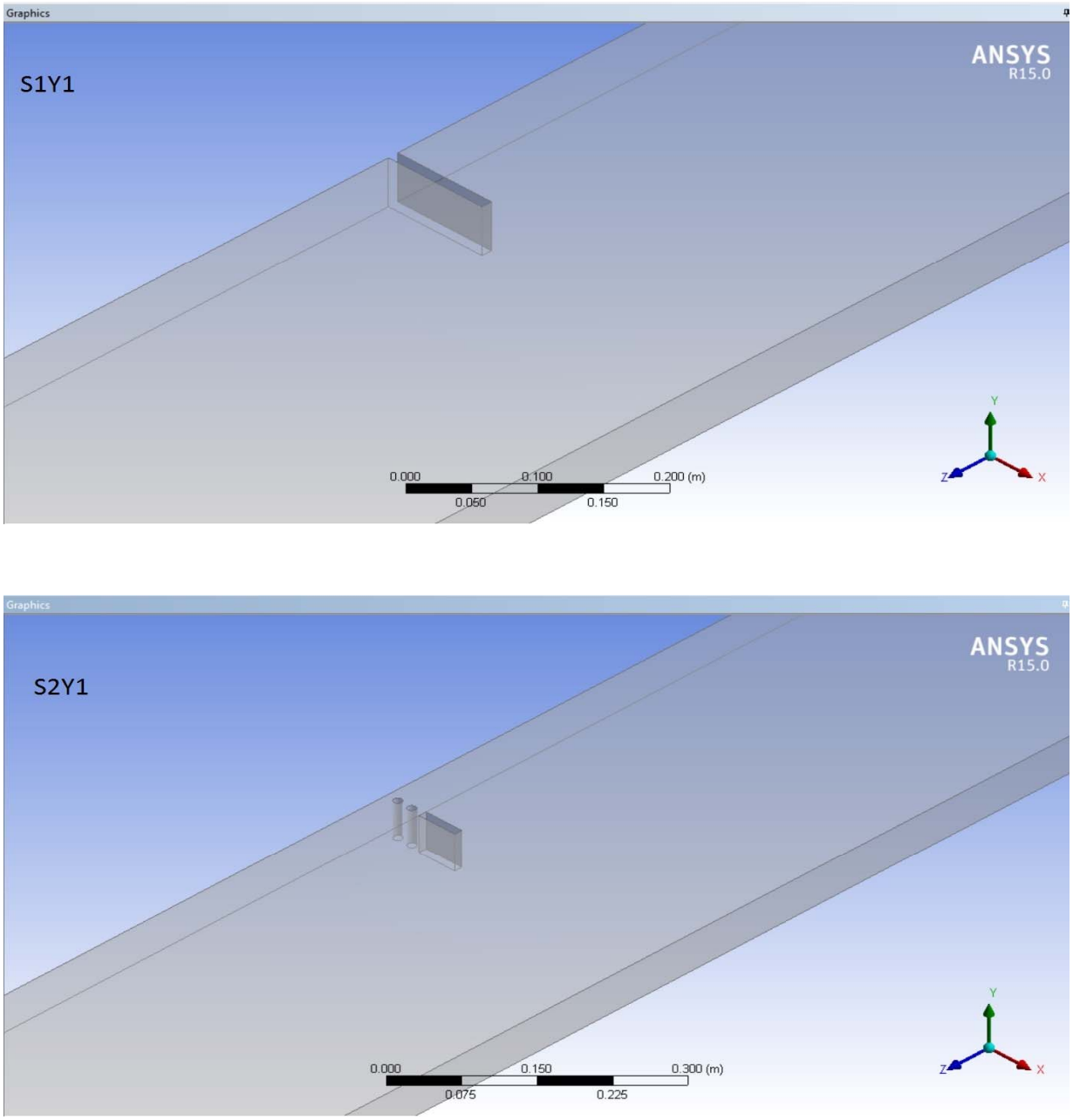

Fig 3.3 Geometry of the numerical model for S1 and S2

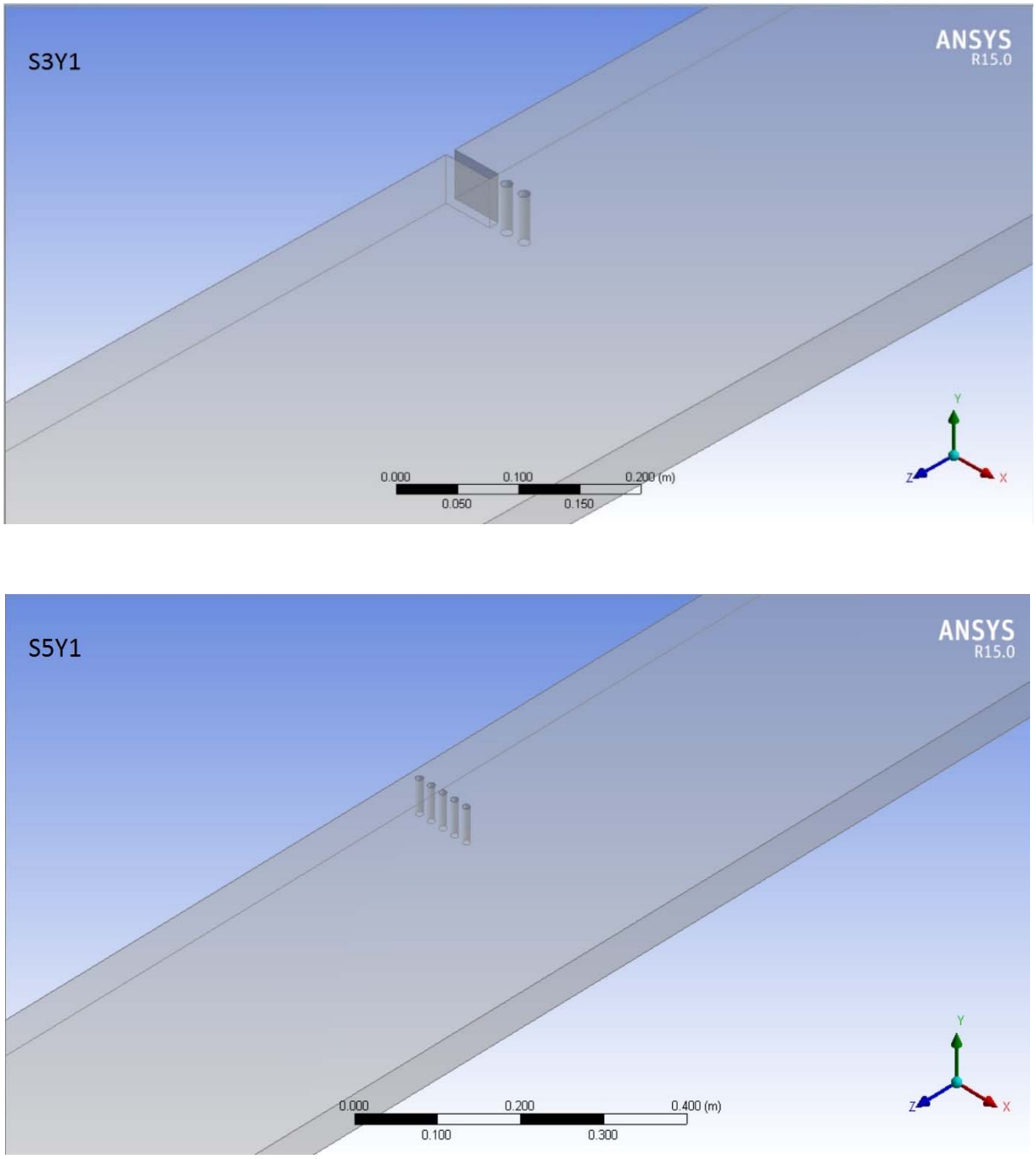

Fig 3.4 Geometry of the numerical model for S3 and S5

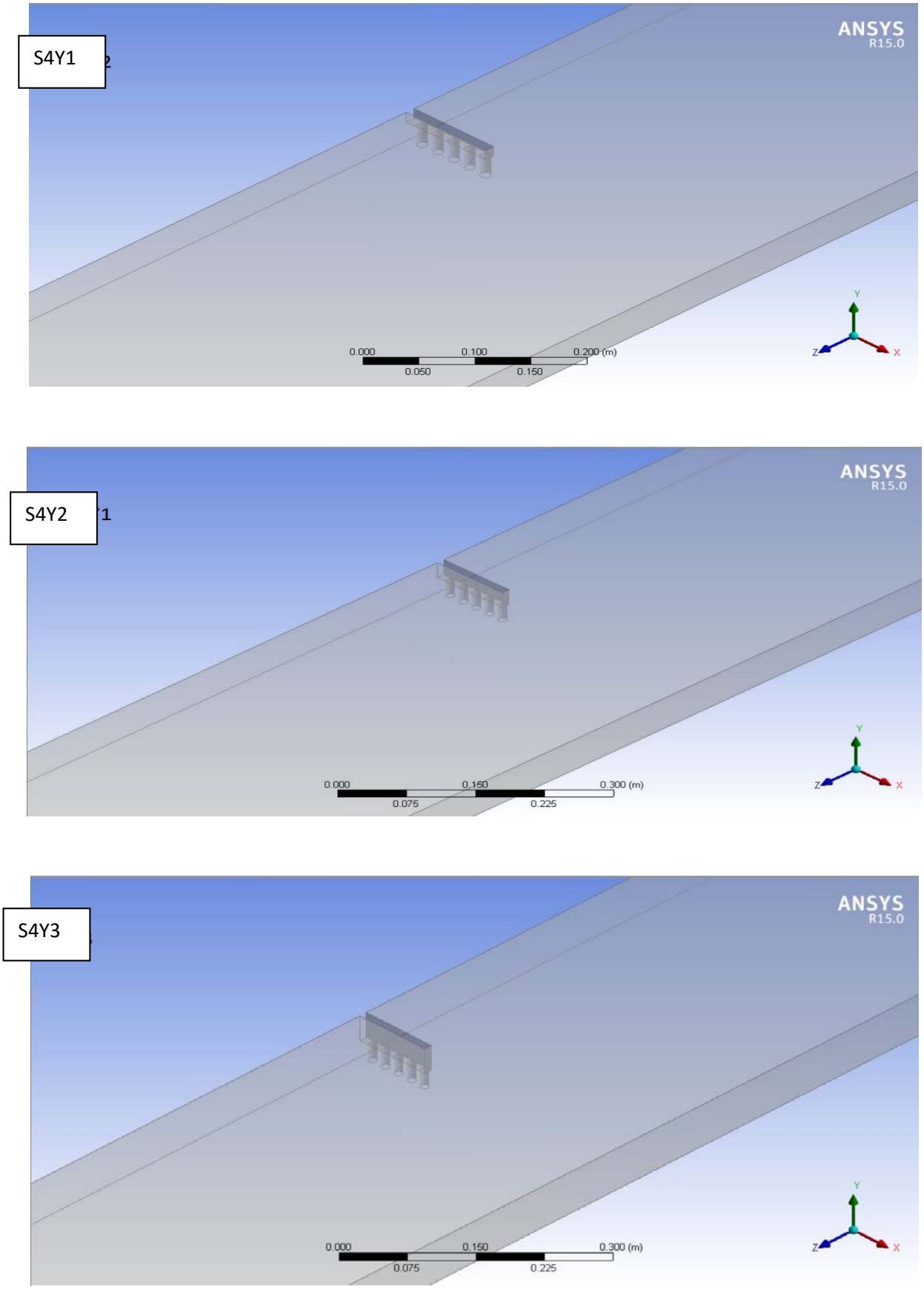

Fig 3.5 Geometry of the numerical model for S4 at different flow depths

3.3.3 Meshing

ANSYS workbench has its own meshing software which generates unstructured mesh. For the present work unstructured mesh with tetrahedral elements is used.

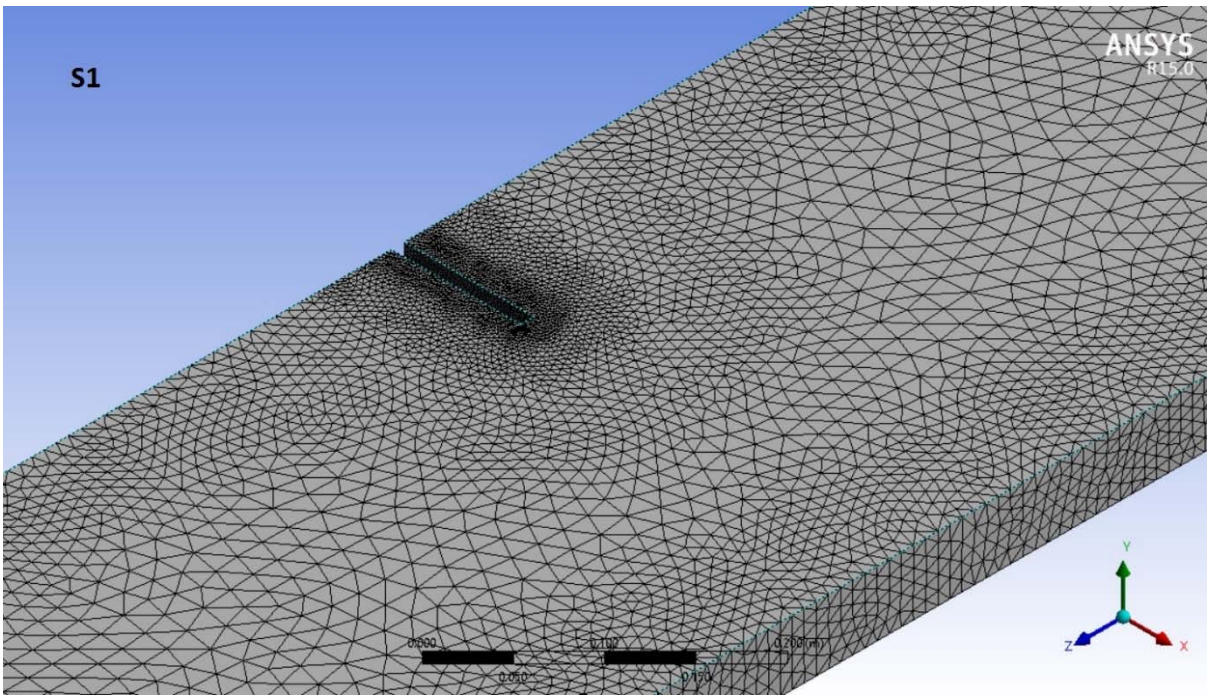

Fig 3.6 Meshing for model spur S1

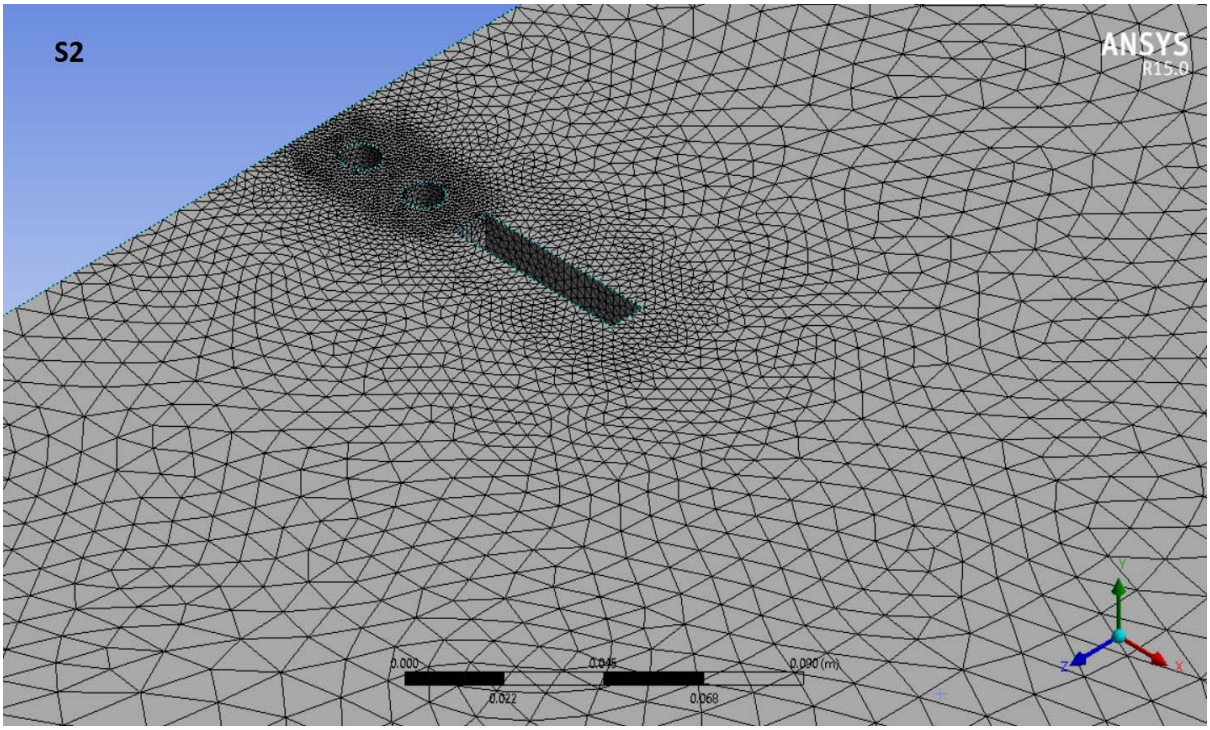

Fig 3.7 Meshing for model spur S2

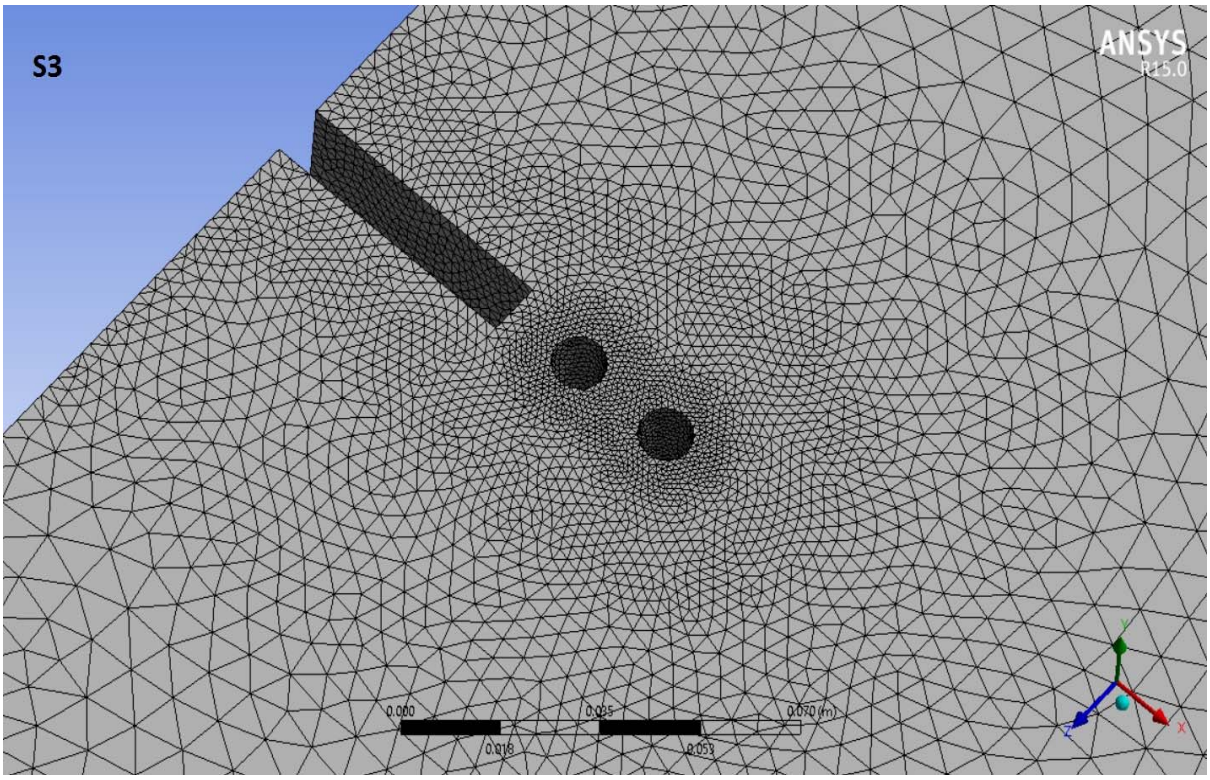

Fig 3.8 Meshing for model spur S3

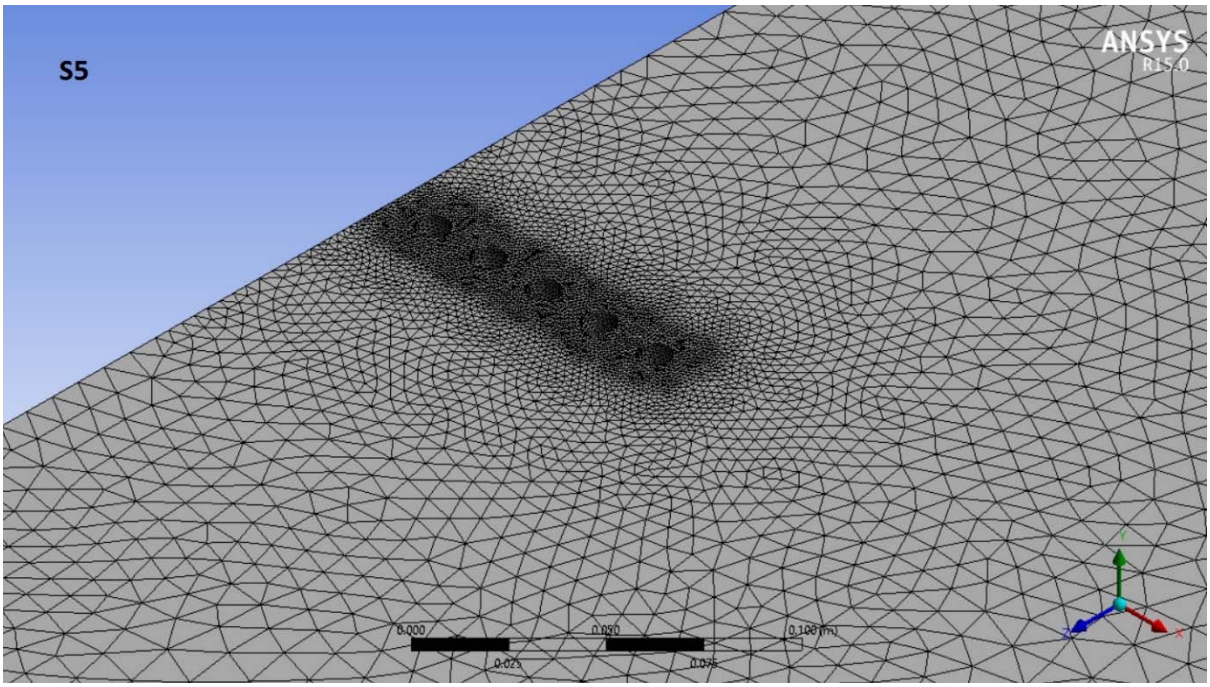

Fig 3.9 Meshing for model spur S5

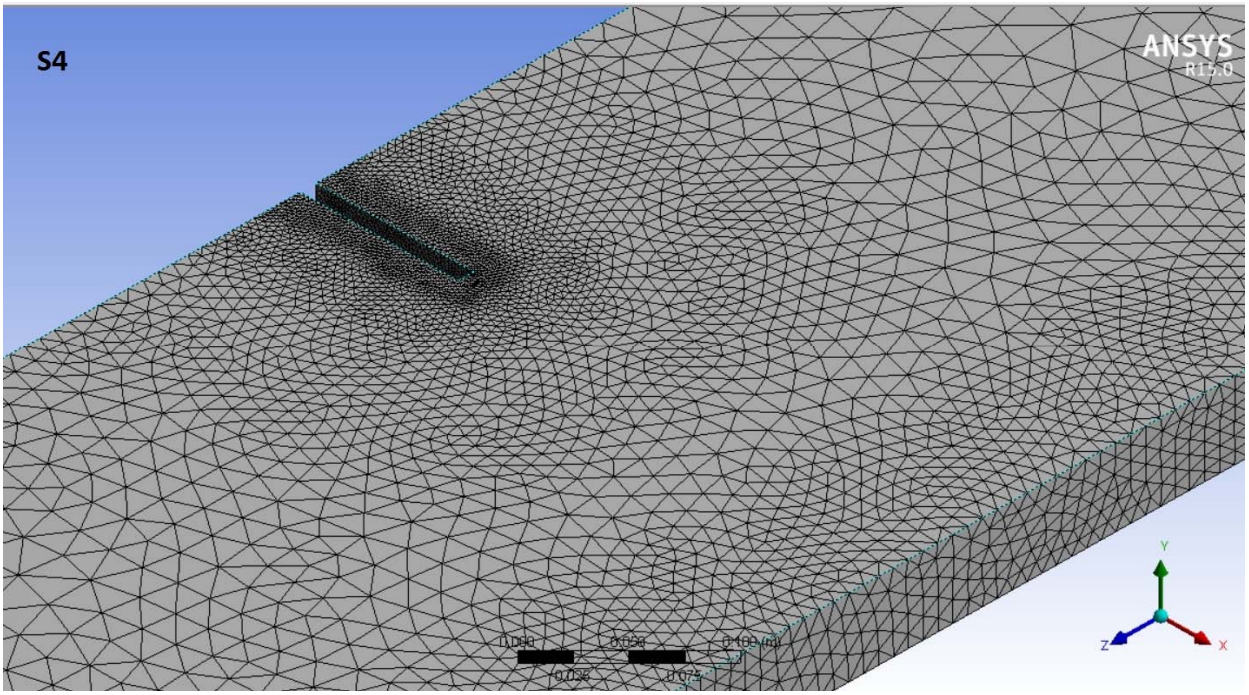

(a)

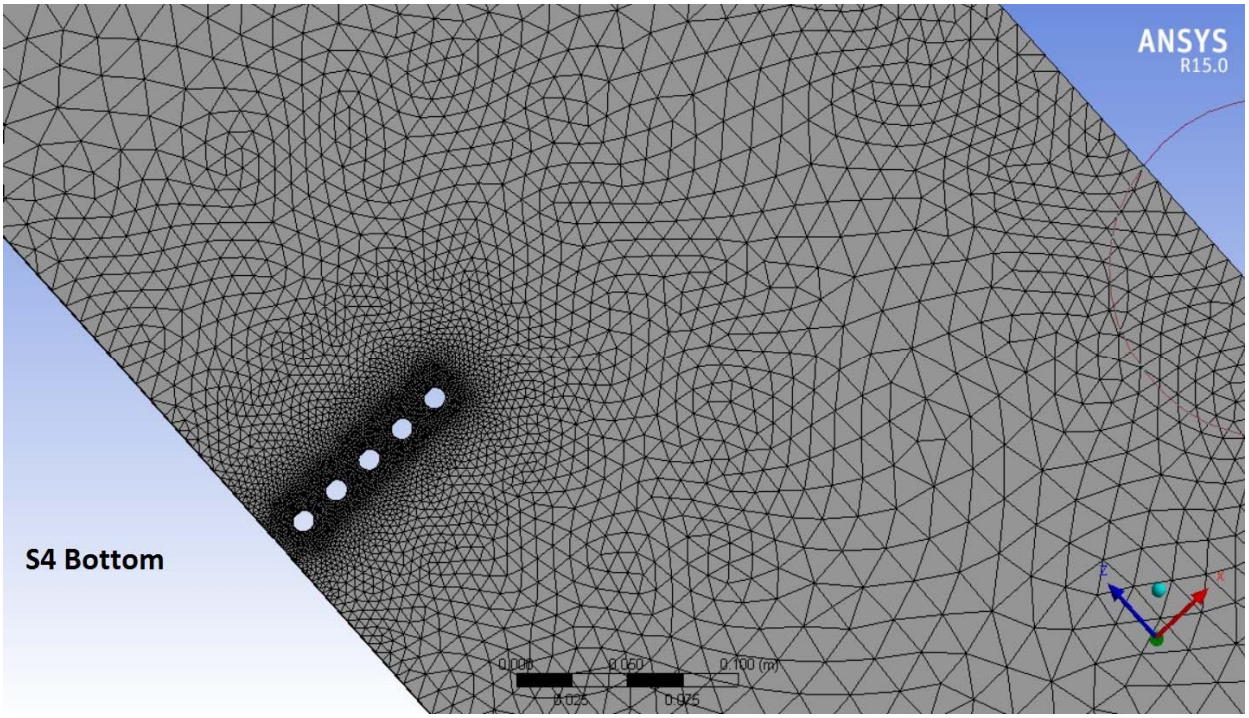

(b)

Fig 3.10 Meshing for model spur S4 (a) top view (b) bottom view

3.3.4 Fluent setup

In the first step gravity is defined in –ve y direction for open channel flow. Realizable k-e model coupled with enhanced wall treatment function for near wall treatment is used in this dissertation work for modelling of turbulent flow around groynes.

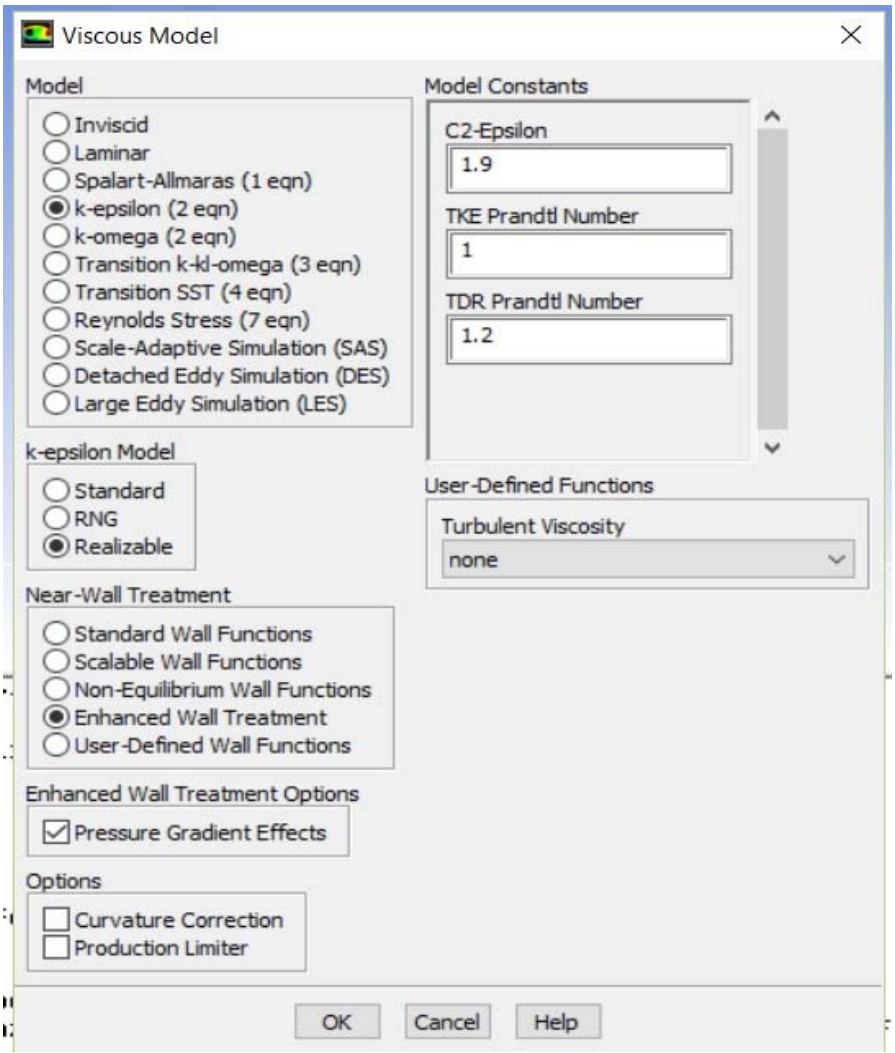

Fig 3.11 viscous models in Fluent

Realizable K-ε model:

The realizable K- ε model differs from the standard K- ε model in two important ways:

- The realizable K- ε model contains an alternative formulation for the turbulent viscosity.
- A modified transport equation for the dissipation rate, ε has been derived from an exact equation for the transport of the mean-square vorticity fluctuation.

The modeled transport equations for K and ε in realizable K- ε model are

$$\frac{\partial}{\partial t}(\rho k) + \frac{\partial}{\partial t}(\rho k u_i) = \frac{\partial}{\partial x_j}\left[\left(\mu + \frac{\mu_t}{\sigma_k}\right)\frac{\partial k}{\partial x_j}\right] + G_k + G_b - \rho\varepsilon - Y_M + S_k$$

And

$$\frac{\partial}{\partial t}(\rho\varepsilon) + \frac{\partial}{\partial t}(\rho\varepsilon u_i) = \frac{\partial}{\partial x_j}\left[\left(\mu + \frac{\mu_t}{\sigma_\varepsilon}\right)\frac{\partial \varepsilon}{\partial x_j}\right] + \rho C_1 S\varepsilon - C_{2\varepsilon}\rho\frac{\varepsilon^2}{k+\sqrt{\nu k}} + C_{1\varepsilon}\frac{\varepsilon}{k}G_b + S_\varepsilon$$

Where, G_k represents the generation of turbulence kinetic energy due to the mean velocity gradients, G_b is the generation of turbulence kinetic energy due to buoyancy. Y_M represents the contribution of the fluctuating dilatation in compressible turbulence to the overall dissipation rate. $C_{1\varepsilon}, and\ C_{2\varepsilon}$ are constants. σ_k and σ_ε are the turbulent Prandtl numbers for k and ε respectively. S_k and S_ε are user-defined source terms.

The turbulent (or eddy) viscosity, μ_t, is computed by combining k and ε as :

$\mu_t = \rho C_\mu \frac{k^2}{\varepsilon}$……Eq.3.3

The difference between the realizable K- ε model and the standard and RNG K- ε models is that C_μ is no longer constant. It is computed from.

$$C_\mu = \frac{1}{A_0 + A_S\frac{kU^*}{\varepsilon}},$$

$$U^* \equiv \sqrt{S_{ij}S_{ij} + \tilde{\Omega}_{ij}\tilde{\Omega}_{ij}},$$

$$\tilde{\Omega}_{ij} = \Omega_{ij} - 2\varepsilon_{ijk}\omega_k$$
$$\Omega_{ij} = \overline{\Omega_{ij}} - \varepsilon_{ijk}\omega_k$$

Where Ω is the mean rate-of-rotation tensor viewed in a moving reference frame with the angular velocity ω_k. The model constants A_0 and As are given by

$$A_0 = 4.04,\ A_S = \sqrt{6}\cos\phi.$$

Where,

$$\phi = \frac{1}{3}\cos^{-1}(\sqrt{6}W),\ W = \frac{S_{ij}S_{jk}S_{ki}}{\tilde{S}^3},\ \tilde{S} = \sqrt{S_{ij}S_{ij}},\ S_{ij} = \frac{1}{2}\left(\frac{\partial u_j}{\partial x_i} + \frac{\partial u_i}{\partial x_j}\right)$$

The model constants $C_{1\varepsilon}, C_{2\varepsilon}, \sigma_k$ and σ_ε have the following default values

$$C_{1\varepsilon} = 1.44,, C_{2\varepsilon} = 1.9, \sigma_k = 1.0, \sigma_\varepsilon = 1.2$$

These default values have been determined from experiments for fundamental turbulent flows including frequently encountered shear flows like boundary layers, mixing layers and jets as well as for decaying isotropic grid turbulence. They have been found to work fairly well for a wide range of wall-bounded and free shear flows.

Cell zone conditions - In the next step materials are defined and cell zone conditions are set as solid for the spur and fluid for the model space.

Boundary conditions: the boundary conditions set are as follows;

Table 3.1 Boundary conditions

Inlet	Velocity inlet
Outlet	Pressure outlet with multiphase open channel flow
Free surface	Symmetry
Bed, channel Walls, and groyne wall	Wall with no slip condition

All surfaces were considered to be hydrodynamically smooth, including the bottom bed.

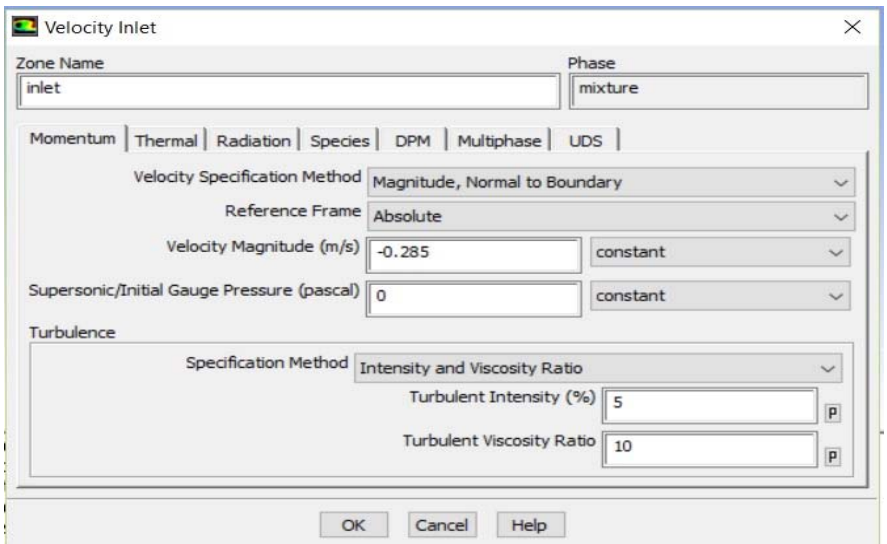

Fig 3.12 Velocity inlet window in Fluent

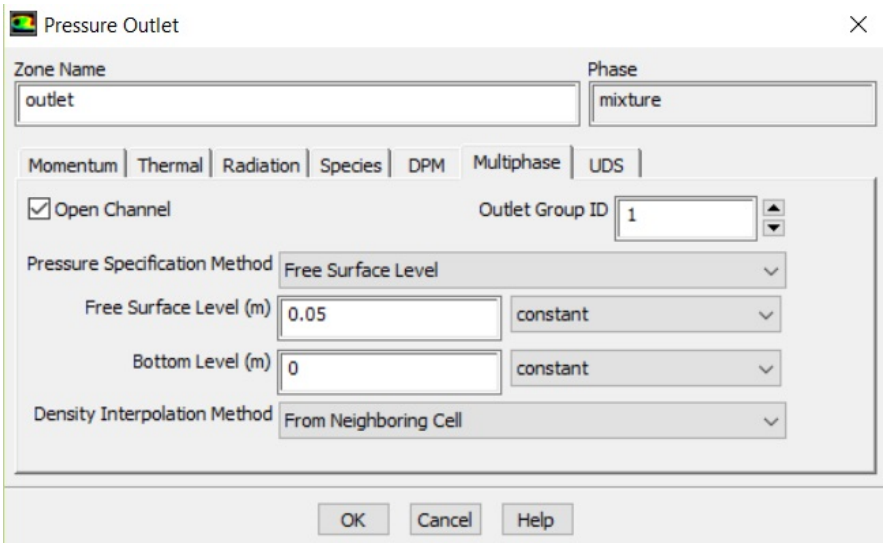

Fig 3.13 Pressure outlet window in Fluent

Solution methods –

The SIMPLE scheme is used for pressure-velocity coupling. Pressure is computed using body force weighted discretisation, second order upwind discretisation is used for turbulence kinetic energy K and dissipation rate ε.

Solution initialisation and calculation -

Reference values are set to be computed from inlet and solution is initialized. Number of iterations is set to 1000 and the solution is calculated to get a converged result.

After the analysis, the results can be viewed in the CFX-POST which also is embedded in ANSYS workbench.

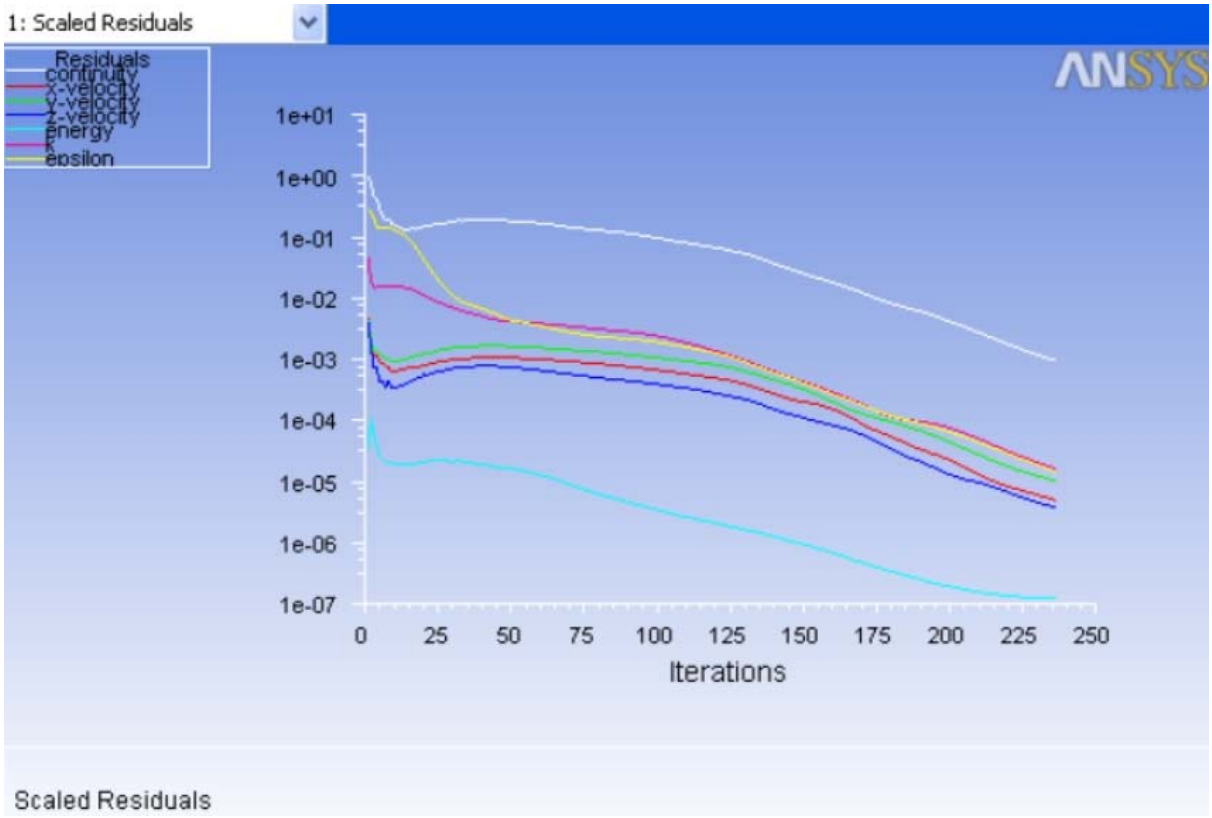

Fig 3.14 Window in fluent during calculations

CHAPTER 4 - NUMERICAL DATA

This chapter contains the data obtained from the Fluent. In total 60 models were analysed for 5 different shape of groyne, 3 flow depth at 4 different Froude number.

4.1 Model validation Data

The experimental work of Yeo et al. is used in this study for the purpose of model validation. The experiment setup is modelled in ANSYS Fluent and numerical data obtained is compared with the experimental data for tip velocity and the percentage error in estimation is found to be well below 10% in all cases.

Table 4.1 Model validation data

Spur	**V_{app}**	**$V_{tip(exp)}$**	**$V_{tip(exp)}$/ V_{app}**	**$V_{tip(num)}$**	**$V_{tip(num)}$/ V_{app}**	**% error in Vtip**
L1P1	0.25	0.31	1.24	0.3	1.2	-3.22581
L2P1	0.25	0.35	1.4	0.337	1.348	-3.71429
L3P1	0.25	0.39	1.56	0.386	1.544	-1.02564
L1P2	0.25	0.31	1.24	0.281	1.124	-9.35484
L2P2	0.25	0.33	1.32	0.303	1.212	-8.18182
L3P2	0.25	0.34	1.36	0.334	1.336	-1.76471
L1P3	0.25	0.3	1.2	0.278	1.112	-7.33333
L2P3	0.25	0.32	1.28	0.297	1.188	-7.1875
L3P3	0.25	0.32	1.28	0.322	1.288	0.625

4.2 Model data:

In this section the numerical analysis data for all models is presented.

4.2.1 Tip velocity data

The data based on tip velocity is shown in the following table. Tip velocity is measured at 70% of flow depth for all cases.

Here,

V_{app} = approach velocity to the spur (m/s),

V_{tip} = velocity at tip of groyne (m/s),

Y = depth of flow (cm)

Table 4.2 numerical data for tip velocity

MODEL	Y(cm)	Froude No.	Vapp (m/s)	Vtip (m/s)	Vtip/Vapp
S1Y1F1	3.75	0.25	0.15	0.23	1.49
S1Y1F2	3.75	0.40	0.25	0.37	1.49
SIY1F3	3.75	0.50	0.30	0.45	1.49
S1Y1F4	3.75	0.75	0.46	0.68	1.50
SIY2F1	5.00	0.25	0.18	0.25	1.42
S1Y2F2	5.00	0.40	0.29	0.44	1.54
S1Y2F3	5.00	0.50	0.35	0.49	1.41
S1Y2F4	5.00	0.75	0.53	0.74	1.41
S1Y3F1	6.25	0.25	0.20	0.29	1.48
S1Y3F2	6.25	0.40	0.32	0.47	1.48
S1Y3F3	6.25	0.50	0.39	0.58	1.49
S1Y3F4	6.25	0.75	0.59	0.89	1.52
S2Y1F1	3.75	0.25	0.15	0.22	1.46
S2Y1F2	3.75	0.40	0.25	0.36	1.48
S2Y1F3	3.75	0.50	0.30	0.45	1.47
S2Y1F4	3.75	0.75	0.46	0.67	1.48
S2Y2F1	5.00	0.25	0.18	0.26	1.50
S2Y2F2	5.00	0.40	0.29	0.42	1.48
S2Y2F3	5.00	0.50	0.35	0.51	1.45
S2Y2F4	5.00	0.75	0.53	0.76	1.45
S2Y3F1	6.25	0.25	0.20	0.29	1.46
S2Y3F2	6.25	0.40	0.32	0.47	1.48
S2Y3F3	6.25	0.50	0.39	0.58	1.47
S2Y3F4	6.25	0.75	0.59	0.85	1.44
S3Y1F1	3.75	0.25	0.15	0.21	1.41
S3Y1F2	3.75	0.40	0.25	0.35	1.42
S3Y1F3	3.75	0.50	0.30	0.43	1.42
S3Y1F4	3.75	0.75	0.46	0.64	1.41
S3Y2F1	5.00	0.25	0.18	0.26	1.46

S3Y2F2	5.00	0.40	0.29	0.41	1.45
S3Y2F3	5.00	0.50	0.35	0.51	1.46
S3Y2F4	5.00	0.75	0.53	0.78	1.48
S3Y3F1	6.25	0.25	0.20	0.28	1.41
S3Y3F2	6.25	0.40	0.32	0.45	1.41
S3Y3F3	6.25	0.50	0.39	0.55	1.41
S3Y3F4	6.25	0.75	0.59	0.83	1.40
S4Y1F1	3.75	0.25	0.15	0.22	1.47
S4Y1F2	3.75	0.40	0.25	0.35	1.41
S4Y1F3	3.75	0.50	0.30	0.44	1.46
S4Y1F4	3.75	0.75	0.46	0.67	1.47
S4Y2F1	5.00	0.25	0.18	0.25	1.45
S4Y2F2	5.00	0.40	0.29	0.39	1.36
S4Y2F3	5.00	0.50	0.35	0.49	1.40
S4Y2F4	5.00	0.75	0.53	0.74	1.40
S4Y3F1	6.25	0.25	0.20	0.29	1.46
S4Y3F2	6.25	0.40	0.32	0.47	1.48
S4Y3F3	6.25	0.50	0.39	0.58	1.49
S4Y3F4	6.25	0.75	0.59	0.88	1.50
S5Y1F1	3.75	0.25	0.15	0.18	1.16
S5Y1F2	3.75	0.40	0.25	0.28	1.15
S5Y1F3	3.75	0.50	0.30	0.36	1.19
S5Y1F4	3.75	0.75	0.46	0.56	1.22
S5Y2F1	5.00	0.25	0.18	0.21	1.17
S5Y2F2	5.00	0.40	0.29	0.35	1.21
S5Y2F3	5.00	0.50	0.35	0.44	1.25
S5Y2F4	5.00	0.75	0.53	0.67	1.28
S5Y3F1	6.25	0.25	0.20	0.23	1.16
S5Y3F2	6.25	0.40	0.32	0.38	1.19
S5Y3F3	6.25	0.50	0.39	0.47	1.20
S5Y3F4	6.25	0.75	0.59	0.70	1.20

4.2.2 Maximum velocity data.

The maximum velocity based data is given in the following table. Here,

V_{max} = maximum velocity attained by flow (m/s),

X = distance from tip across the direction of flow (m),

Z = distance from tip in the direction of flow (m).

The negative values of X indicates that the location is towards the bank on which groyne is installed.

Table 4.3 Numerical data for maximum velocity

MODEL	Vapp (m/s)	Vmax(m/s)	Vmax/Vapp	z (m)	X(m)
S1Y1F1	0.1516	0.3088	2.0369	0.5690	0.1410
S1Y1F2	0.2468	0.5210	2.1110	0.5510	0.1487
SIY1F3	0.3032	0.6460	2.1306	0.5130	0.1431
S1Y1F4	0.4550	0.9838	2.1622	0.4944	0.1530
SIY2F1	0.1751	0.3760	2.1473	0.5245	0.1830
S1Y2F2	0.2860	0.6350	2.2203	-0.4790	0.1486
S1Y2F3	0.3500	0.7860	2.2457	0.5075	0.1846
S1Y2F4	0.5253	1.2100	2.3034	0.4763	0.1710
S1Y3F1	0.1958	0.4300	2.1966	0.5146	0.1472
S1Y3F2	0.3187	0.7400	2.3219	0.5015	0.1616
S1Y3F3	0.3915	0.9100	2.3244	0.5015	0.1616
S1Y3F4	0.5872	1.4200	2.4183	0.4588	0.1508
S2Y1F1	0.2468	0.4800	1.9449	0.0002	-0.0710
S2Y1F2	0.1516	0.2900	1.9129	0.0015	-0.0707
S2Y1F3	0.3032	0.6600	2.1768	0.0002	-0.0710
S2Y1F4	0.4550	1.0200	2.2418	0.0007	-0.0710
S2Y2F1	0.1751	0.3500	1.9989	-0.0011	-0.0585
S2Y2F2	0.2860	0.5800	2.0280	-0.0008	-0.0790
S2Y2F3	0.3500	0.7400	2.1143	0.0010	-0.0710
S2Y2F4	0.5253	1.1200	2.1321	-0.0018	-0.0700
S2Y3F1	0.1958	0.4223	2.1572	-0.0014	-0.0592
S2Y3F2	0.3187	0.6896	2.1638	-0.0019	-0.0590

S2Y3F3	0.3915	0.8582	2.1921	0.0008	-0.0707
S2Y3F4	0.5872	1.3088	2.2289	0.0017	-0.0710
S3Y1F1	0.1516	0.3118	2.0567	0.0006	-0.0208
S3Y1F2	0.2468	0.5127	2.0774	-0.0025	-0.0097
S3Y1F3	0.3032	0.6350	2.0943	-0.0028	-0.0100
S3Y1F4	0.4550	0.9651	2.1211	0.0025	-0.0098
S3Y2F1	0.1751	0.3523	2.0120	0.0007	-0.0208
S3Y2F2	0.2860	0.5898	2.0622	-0.0015	-0.0206
S3Y2F3	0.3500	0.7295	2.0843	0.0010	-0.0206
S3Y2F4	0.5253	1.1085	2.1102	0.0010	-0.0206
S3Y3F1	0.1958	0.4005	2.0459	0.0011	-0.0206
S3Y3F2	0.3187	0.6680	2.0960	0.0028	-0.0100
S3Y3F3	0.3915	0.8229	2.1019	0.0008	-0.0206
S3Y3F4	0.5872	1.2840	2.1866	-0.0023	-0.0100
S4Y1F1	0.1516	0.2970	1.9588	-0.0011	-0.0107
S4Y1F2	0.2468	0.4917	1.9923	-0.0011	-0.0107
S4Y1F3	0.3032	0.6022	1.9860	-0.0010	-0.0107
S4Y1F4	0.4550	0.9159	2.0130	-0.0010	-0.0108
S4Y2F1	0.1751	0.3200	1.8275	-0.0010	-0.0107
S4Y2F2	0.2860	0.4850	1.6958	-0.0008	-0.0100
S4Y2F3	0.3500	0.6600	1.8857	-0.0007	-0.0107
S4Y2F4	0.5253	1.0300	1.9608		0.1000
S4Y3F1	0.1958	0.3756	1.9187	-0.0009	-0.0107
S4Y3F2	0.3187	0.6139	1.9263	-0.0014	-0.0110
S4Y3F3	0.3915	0.7500	1.9157	-0.0014	-0.0110
S4Y3F4	0.5872	1.1640	1.9823	0.0023	-0.0100
S5Y1F1	0.1516	0.2300	1.5172	0.0044	-0.0305
S5Y1F2	0.2468	0.4100	1.6613	0.0044	-0.0305
S5Y1F3	0.3032	0.5400	1.7810	0.0046	-0.0500
S5Y1F4	0.4550	0.8740	1.9209	0.0046	-0.0500
S5Y2F1	0.1751	0.3060	1.7476	0.0044	-0.0191

S5Y2F2	0.2860	0.4800	1.6783	0.0051	-0.0373
S5Y2F3	0.3500	0.6140	1.7543	0.0047	-0.0304
S5Y2F4	0.5253	0.9830	1.8713	0.0047	-0.0305
S5Y3F1	0.1958	0.3580	1.8288	0.0049	-0.0104
S5Y3F2	0.3187	0.5480	1.7195	0.0049	-0.0104
S5Y3F3	0.3915	0.7450	1.9029	0.0042	-0.0191
S5Y3F4	0.5872	1.1400	1.9414	0.0049	-0.0300
S5Y2F3	0.3032	0.5400	1.7810	0.0046	-0.0500
S5Y2F4	0.4550	0.8740	1.9209	0.0046	-0.0500
S5Y3F1	0.3187	0.5480	1.7195	0.0049	-0.0104
S5Y3F2	0.1958	0.3580	1.8288	0.0049	-0.0104
S5Y3F3	0.3915	0.7450	1.9029	0.0042	-0.0191
S5Y3F4	0.5872	1.1400	1.9414	0.0049	-0.0300

4.2.3 Maximum bed shear stress (τ_m) data

In the following table values based on maximum bed shear stress (τ_m) and bed shear stress of undisturbed flow (τ_0) is presented. The maximum bed shear stress (τ_m) is found near the tip of groyne in almost all cases.

Here,

τ_0 = Bed shear stress of undisturbed flow on the centreline before the installation of spur (Pa),

τ_m = maximum bed shear stress (Pa).

τ_m/τ_0 = shear stress amplification factor.

Table 4.4 Values of bed shear stress and shear amplification factor

MODEL	τ_0 (Pa)	τ_m (Pa)	τ_m/τ_0
S1Y1F1	0.34	1.64	4.82
S1Y1F2	0.63	2.975	4.72
S1Y1F3	0.82	3.819	4.66
S1Y1F4	1.4	7.12	5.09
S1Y2F1	0.24	1.406	5.86
S1Y2F2	0.47	2.9	6.17
S1Y2F3	0.63	4.139	6.57
S1Y2F4	1.34	9.085	6.78
S1Y3F1	0.28	1.932	6.9
S1Y3F2	0.59	4.148	7.03
S1Y3F3	0.83	5.943	7.16
S1Y3F4	1.66	12.18	7.34
S2Y1F1	0.34	1.1	3.24
S2Y1F2	0.63	2.865	4.55
S2Y1F3	0.82	4.25	5.18
S2Y1F4	1.4	9.25	6.61
S2Y2F1	0.24	1.339	5.58
S2Y2F2	0.47	2.994	6.37
S2Y2F3	0.63	4.145	6.58
S2Y2F4	1.34	9.152	6.83
S2Y3F1	0.28	1.831	6.54

S2Y3F2	0.59	4.295	7.28
S2Y3F3	0.83	5.921	7.13
S2Y3F4	1.66	11.1	6.69
S3Y1F1	0.34	1.12	3.29
S3Y1F2	0.63	2.656	4.22
S3Y1F3	0.82	3.859	4.71
S3Y1F4	1.4	7.23	5.16
S3Y2F1	0.24	1.108	4.62
S3Y2F2	0.47	2.145	4.56
S3Y2F3	0.63	3.355	5.33
S3Y2F4	1.34	7.55	5.63
S3Y3F1	0.28	1.508	5.39
S3Y3F2	0.59	3.476	5.89
S3Y3F3	0.83	4.627	5.57
S3Y3F4	1.66	9.46	5.7
S4Y1F1	0.34	1.08	3.18
S4Y1F2	0.63	2.157	3.42
S4Y1F3	0.82	3.418	4.17
S4Y1F4	1.4	6.23	4.45
S4Y2F1	0.24	0.785	3.27
S4Y2F2	0.47	1.983	4.22
S4Y2F3	0.63	2.772	4.4
S4Y2F4	1.34	6.124	4.57
S4Y3F1	0.28	1.316	4.7
S4Y3F2	0.59	3.009	5.1
S4Y3F3	0.83	4.499	5.42
S4Y3F4	1.66	9.362	5.64
S5Y1F1	0.34	0.874	2.57
S5Y1F2	0.63	2.147	3.41
S5Y1F3	0.82	2.967	3.62
S5Y1F4	1.4	5.87	4.19

S5Y2F1	0.24	0.718	2.99
S5Y2F2	0.47	1.521	3.24
S5Y2F3	0.63	2.394	3.8
S5Y2F4	1.34	5.15	3.84
S5Y3F1	0.28	1.154	4.12
S5Y3F2	0.59	2.328	3.95
S5Y3F3	0.83	3.874	4.67
S5Y3F4	1.66	7.83	4.72

4.2.4 Separation length data

The numerically obtained values of separation length is given in the following table. Here,

L_{sep} =separation length obtained numerically (m),

L=length of spur in m.

Table 4.5 Values of separation length

MODEL	Vapp (m/s)	sep length (m)	L (m)	Lsep/L
S1Y1F1	0.18	1.08	0.1	10.8
S1Y1F2	0.285	1.13	0.1	11.3
SIY1F3	0.35	1.091	0.1	10.91
S1Y1F4	0.5253	1.06	0.1	10.6
SIY2F1	0.15	1.18	0.1	11.8
S1Y2F2	0.25	1.21	0.1	12.1
S1Y2F3	0.3	1.25	0.1	12.5
S1Y2F4	0.455	1.27	0.1	12.7
S1Y3F1	0.195	1.075	0.1	10.75
S1Y3F2	0.38	1.046	0.1	10.46
S1Y3F3	0.39	1.016	0.1	10.16
S1Y3F4	0.59	1.055	0.1	10.55
S2Y1F1	0.18	0.504	0.1	5.04
S2Y1F2	0.285	0.5347	0.1	5.347
S2Y1F3	0.35	0.5655	0.1	5.655
S2Y1F4	0.53	0.4232	0.1	4.232
S2Y2F1	0.15	0.493	0.1	4.93
S2Y2F2	0.25	0.54	0.1	5.4
S2Y2F3	0.3	0.56	0.1	5.6
S2Y2F4	0.455	0.596	0.1	5.96
S2Y3F1	0.195	0.4933	0.1	4.933
S2Y3F2	0.38	0.4618	0.1	4.618
S2Y3F3	0.39	0.548	0.1	5.48
S2Y3F4	0.59	0.58	0.1	5.8
S3Y1F1	0.18	0.55	0.1	5.5

S3Y1F2	0.285	0.66	0.1	6.6
S3Y1F3	0.35	0.566	0.1	5.66
S3Y1F4	0.5253	0.505	0.1	5.05
S3Y2F1	0.15	0.3952	0.1	3.952
S3Y2F2	0.25	0.3923	0.1	3.923
S3Y2F3	0.3	0.3642	0.1	3.642
S3Y2F4	0.455	0.3763	0.1	3.763
S3Y3F1	0.195	0.44	0.1	4.4
S3Y3F2	0.38	0.465	0.1	4.65
S3Y3F3	0.39	0.476	0.1	4.76
S3Y3F4	0.59	0.49	0.1	4.9
S4Y1F1	0.18	0.7298	0.1	7.298
S4Y1F2	0.285	0.7948	0.1	7.948
S4Y1F3	0.35	0.81	0.1	8.1
S4Y1F4	0.5253	0.8427	0.1	8.427
S4Y2F1	0.15	0.74	0.1	7.4
S4Y2F2	0.25	0.788	0.1	7.88
S4Y2F3	0.3	0.801	0.1	8.01
S4Y2F4	0.455	0.813	0.1	8.13
S4Y3F1	0.195	0.7837	0.1	7.837
S4Y3F2	0.38	0.804	0.1	8.04
S4Y3F3	0.39	0.8261	0.1	8.261
S4Y3F4	0.59	0.8284	0.1	8.284
S5Y1F1	0.18	-	0.1	-
S5Y1F2	0.285	-	0.1	-
S5Y1F3	0.35	-	0.1	-
S5Y1F4	0.5253	-	0.1	-
S5Y2F1	0.15	-	0.1	-
S5Y2F2	0.25	-	0.1	-
S5Y2F3	0.3	-	0.1	-
S5Y2F4	0.455	-	0.1	-

S5Y3F1	0.195	-	0.1	-
S5Y3F2	0.38	-	0.1	-
S5Y3F3	0.39	-	0.1	-
S5Y3F4	0.59	-	0.1	-

CHAPTER 5-RESULTS AND DISCUSSIONS

5.1 Model validation result

In this section the results of numerical model for experimental setup of Yeo et al.(10) is compared with the experimental result obtained by them for validation of model. The values of tip velocity obtained numerically are compared with experimental values of tip velocity.

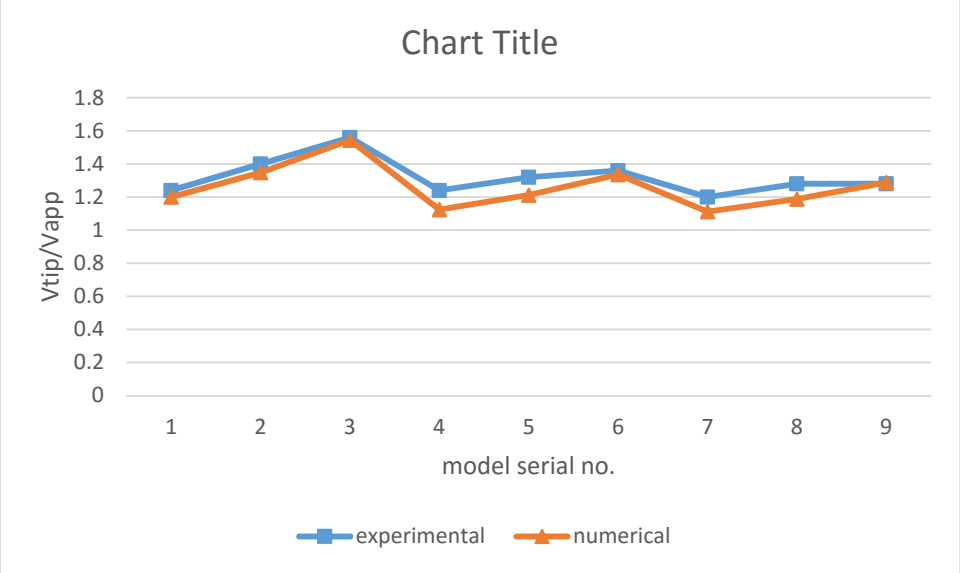

Fig 5.1 comparison of experimental and numerical values of tip velocity

For model validation

5.2 Results based on Tip velocity

Here the results based on tip velocity are presented. Flow at the tip of spur dyke is highly turbulent and changes abruptly towards the centre of channel forming intensive vortex near the tip, which leads to high local scour. The tip velocity was measured at the middle layer (70% of the water depth).

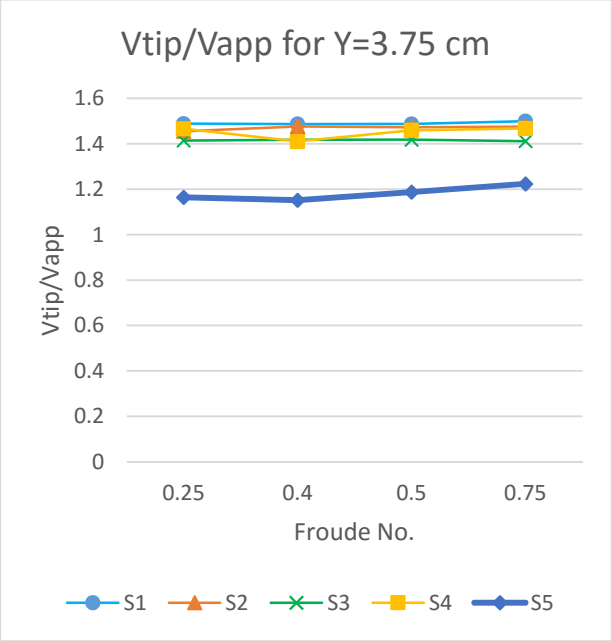

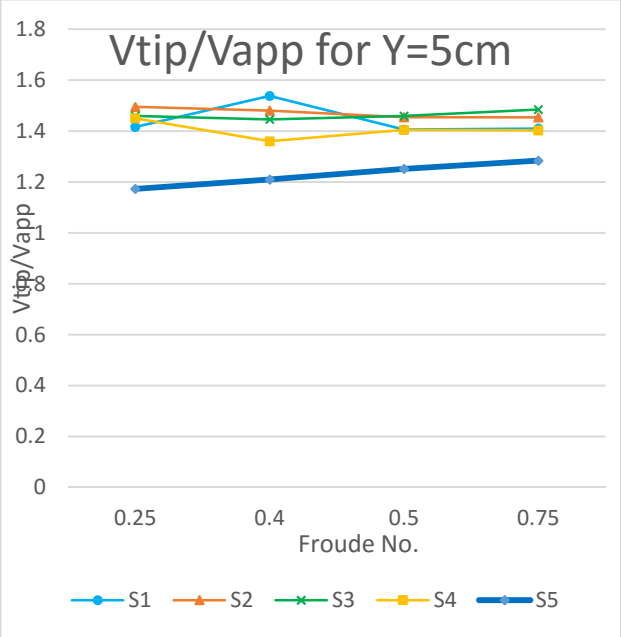

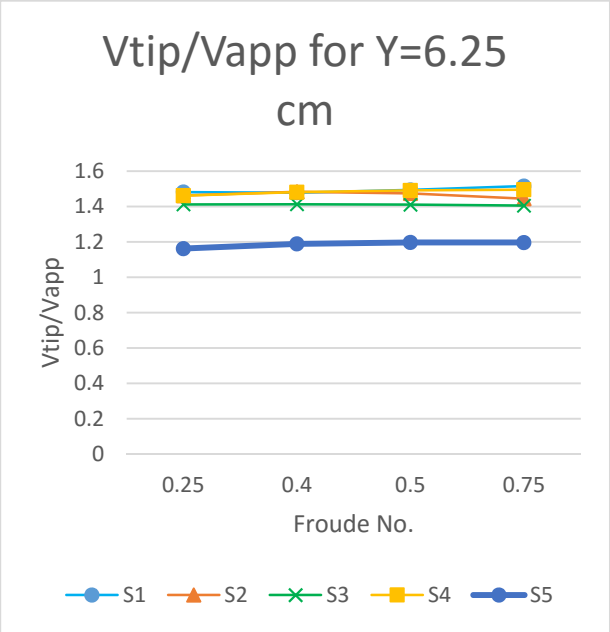

Fig 5.2 variation of tip velocity with Froude no. at different flow depth.

The above plots show that tip velocity is maximum for impermeable structure and minimum for spur 5 ie permeable spur. The tip velocity for spur type 3 is also found lower than other spur. Froude no seems to have little effect on tip velocity in any case.

5.3 Results based on maximum velocity

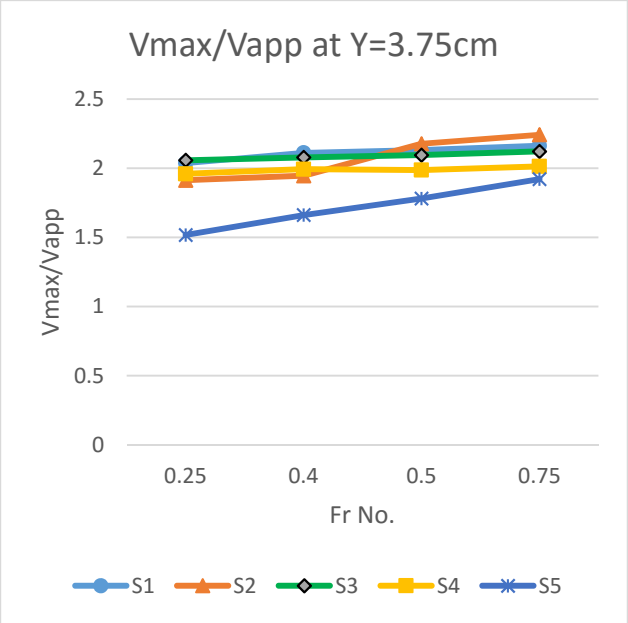

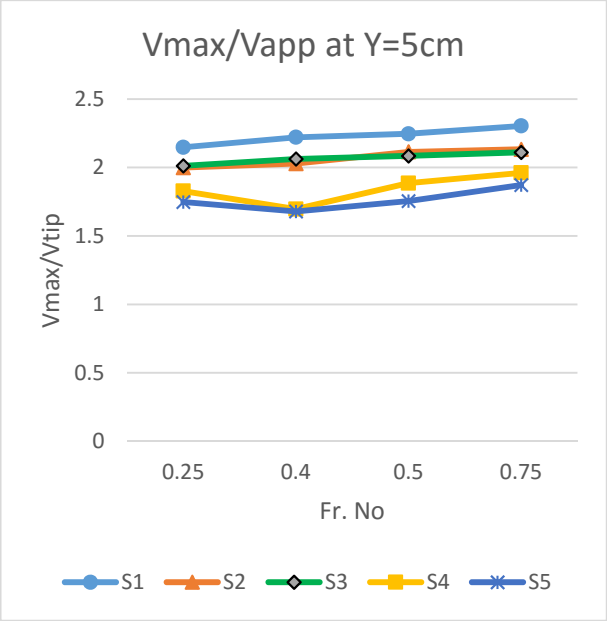

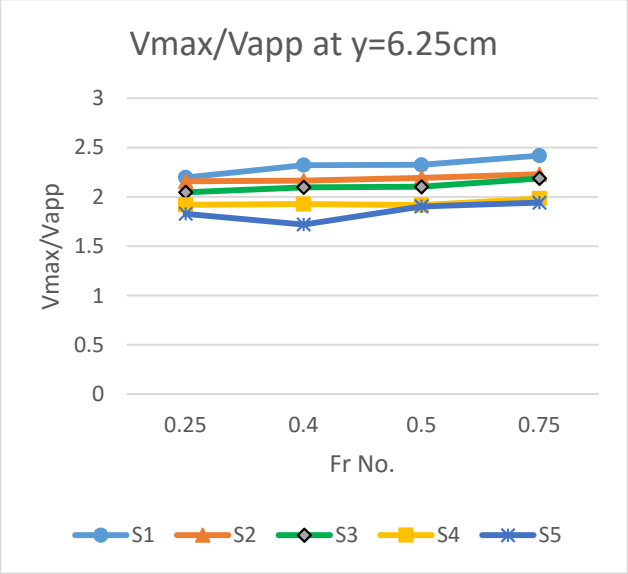

Fig 5.3 variation of maximum velocity with Froude no. at different flow depth.

The graphs show the variation of velocity amplification factor for flow at different Froude number for different hybrid groynes considered. The graph shows that permeable groyne have least velocity amplification factor followed by bandall like structure. While the performance of structure with permeable root is found poorest in controlling velocity amplification. Froude number is found to have little or no effect on velocity amplification however the value of velocity amplification factor is found to increase slightly with increase in Froude number for all cases.

5.4 Results based on separation length.

This section contains results based on the separation length obtained from numerical data. The ratio of separation length to the spur length is compared at different Froude number for all the considered structures.

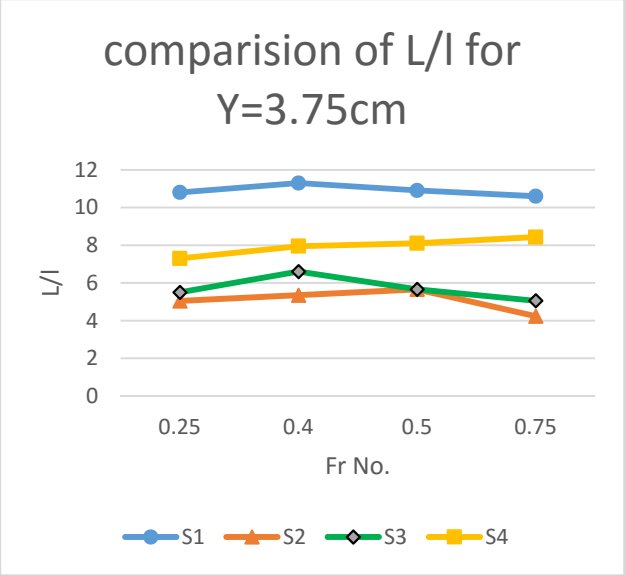

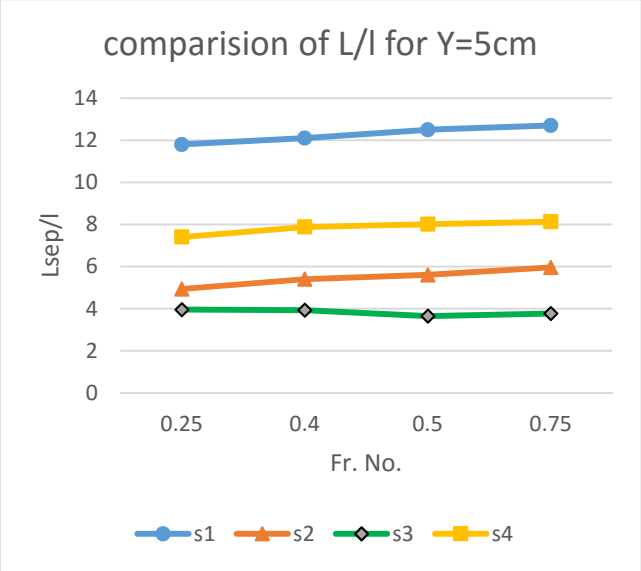

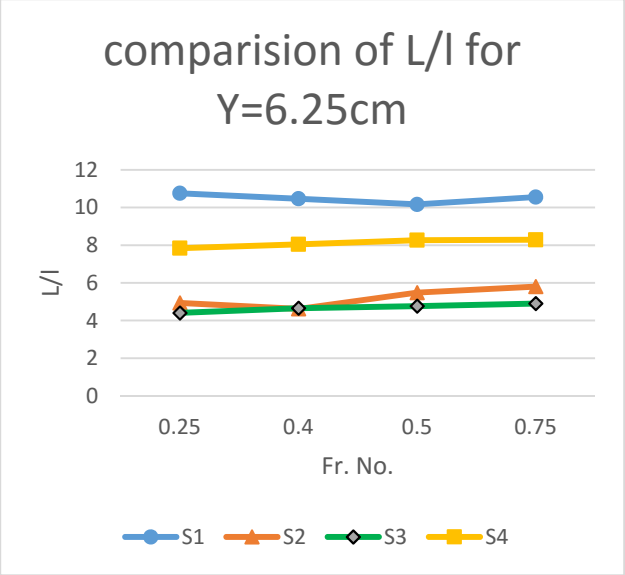

Fig 5.4 variation of separation length with Froude no. at different flow depth

The above graphs show the variation of separation length for all the spurs. From the plots it is clear that impermeable groyne gives the largest separation length as compared to any other spur with the bandall spur also providing a good value of separation length, the performance of S3 and S4 is found to be nearly half of that of impermeable one and is considered poor. The separation length shows little variation with Froude number.

5.5 Results based on maximum bed shear stress

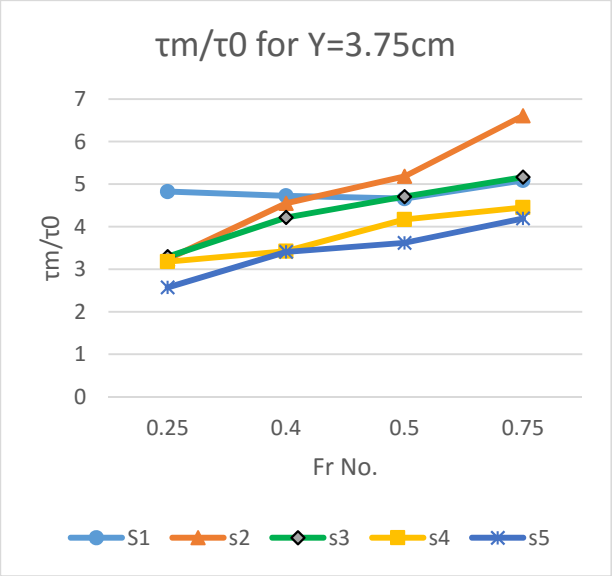

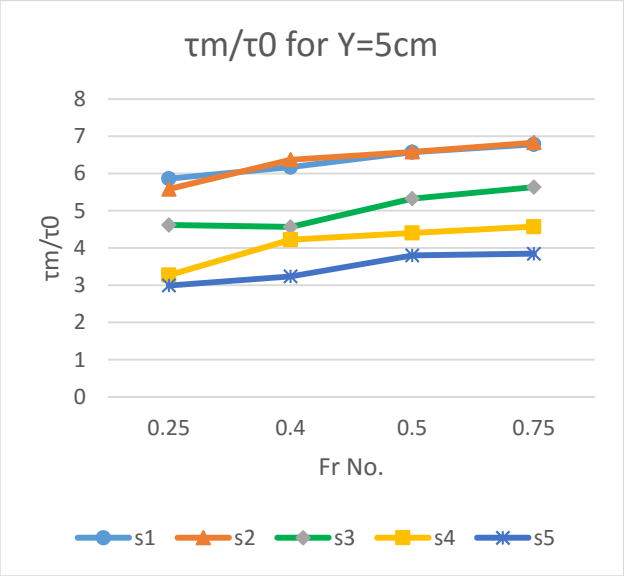

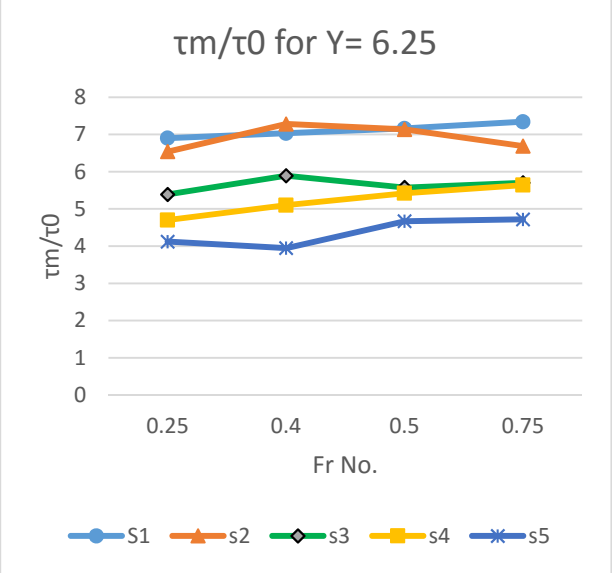

Fig 5.5 variation of shear amplification factor with Froude number for different flow depths.

The above plots show the variation of bed shear stress amplification for the spurs at varying Froude number. The shear stress amplification increases with increase in Froude number in all the cases. From the plots it is clear that shear amplification is highest for impermeable spur1 and spur 2 which is permeable at root. From the above plots it can be seen that bandall structure works considerably well in reducing the shear stress at bed. The spur with permeable tip also shows considerable drop in bed shear stress.

5.6 Results based on separation length and maximum bed shear stress

To check the performance of the spurs a parameter based on bed shear amplification factor and separation length is used. The ratio of L/l to τ_m/τ_0 for all the models is computed and compared.

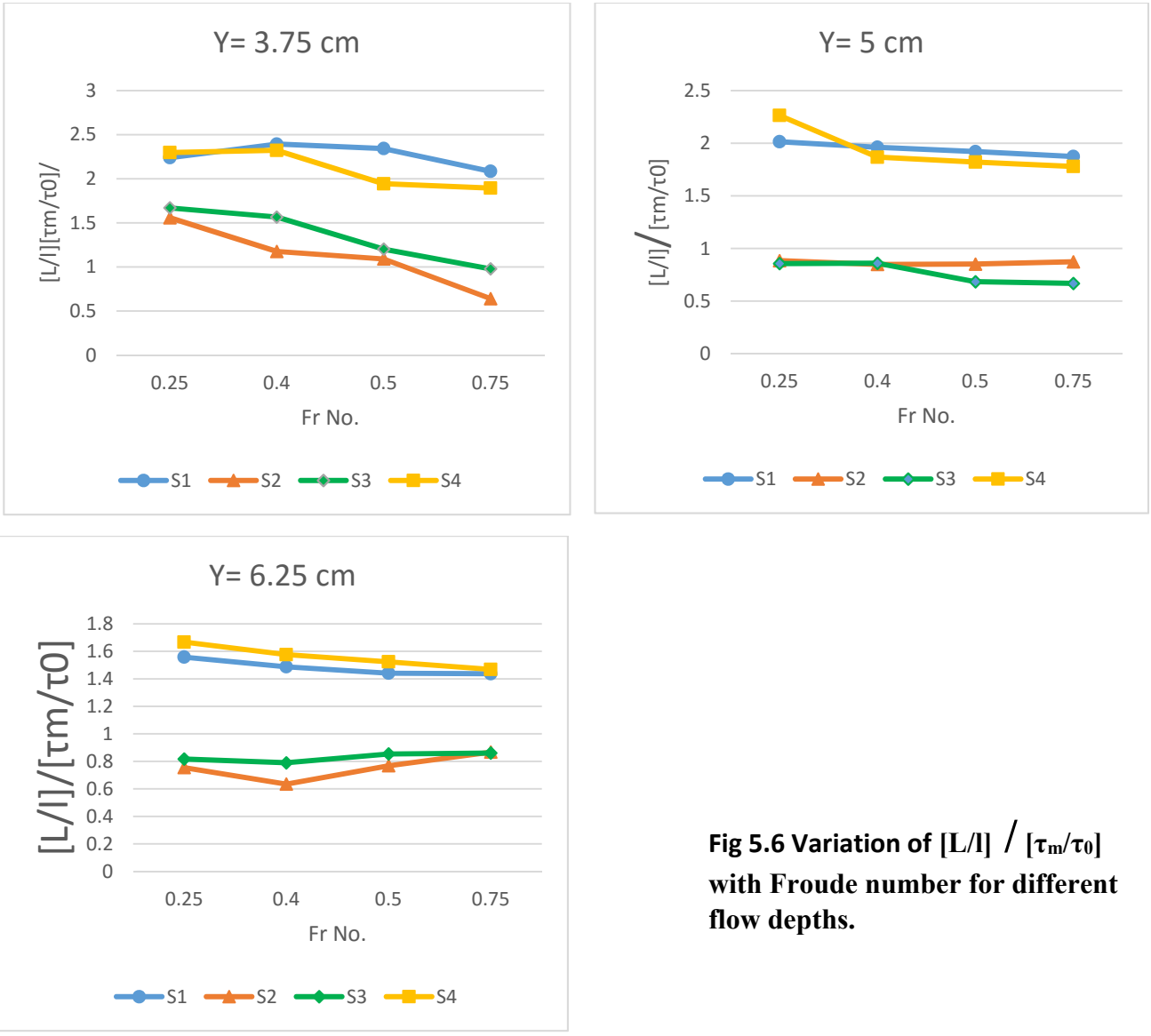

Fig 5.6 Variation of [L/l] / [τ_m/τ_0] with Froude number for different flow depths.

The above plots show that spur4 and spur 5 shows nearly similar behaviour on this parameter. The values of [L/l]/[τm/τ0] decreases with increase in Froude number. It can also be seen that the spur dyke S4 and S5 shows the highest values on this parameter. So it can be said that spur dyke S4 (Bandall structure) gives performance nearly similar to impermeable groyne.

5.7 Results based on separation length and Velocity amplification

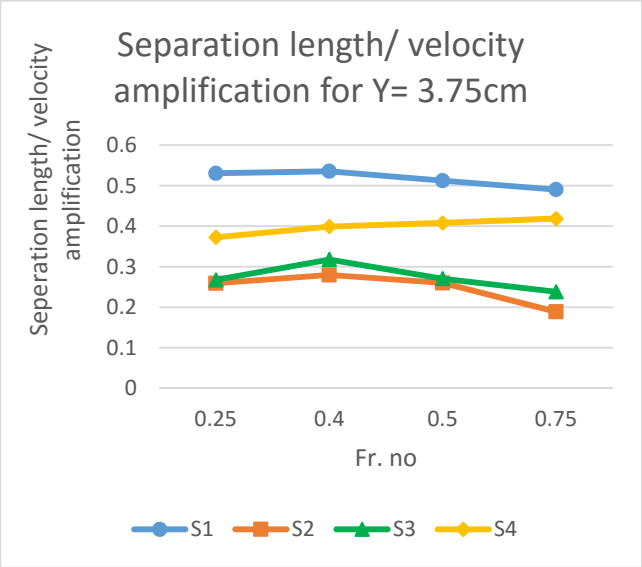

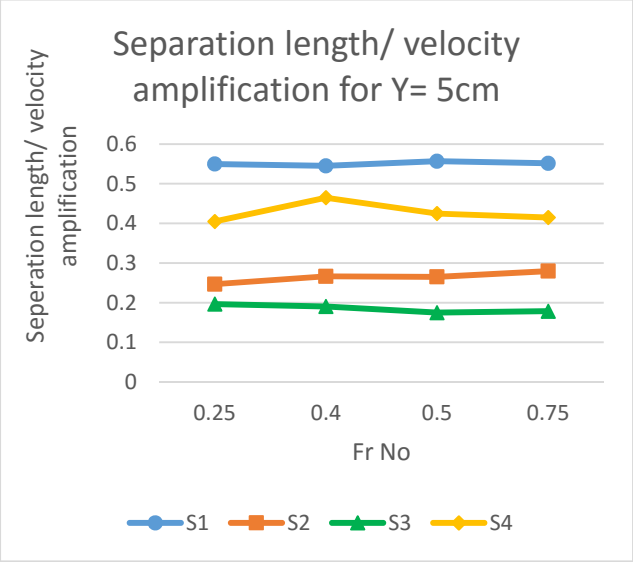

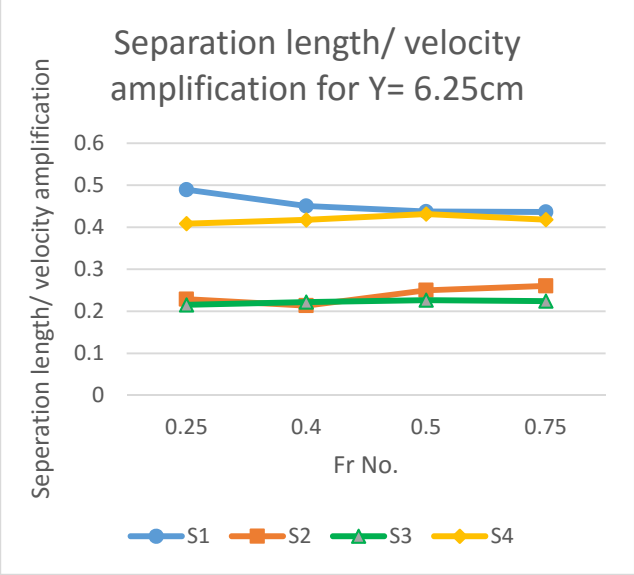

Fig 5.7 Variation of Separation length/ velocity amplification with Froude number for different flow depth.

The above plots show the variation of ratio of separation length and velocity amplification with Froude number for different flow depths. The plots show that impermeable groyne gives best separation length velocity amplification ratio. The spur4 also shows high value of separation length velocity amplification ratio. These plots show that spur4 can be used as replacement for impermeable spur.

5.8 Software plots

This section contains the plots contour diagrams of bed shear stress and velocity, and streamlines of flow.

5.8.1 Velocity contour diagrams.

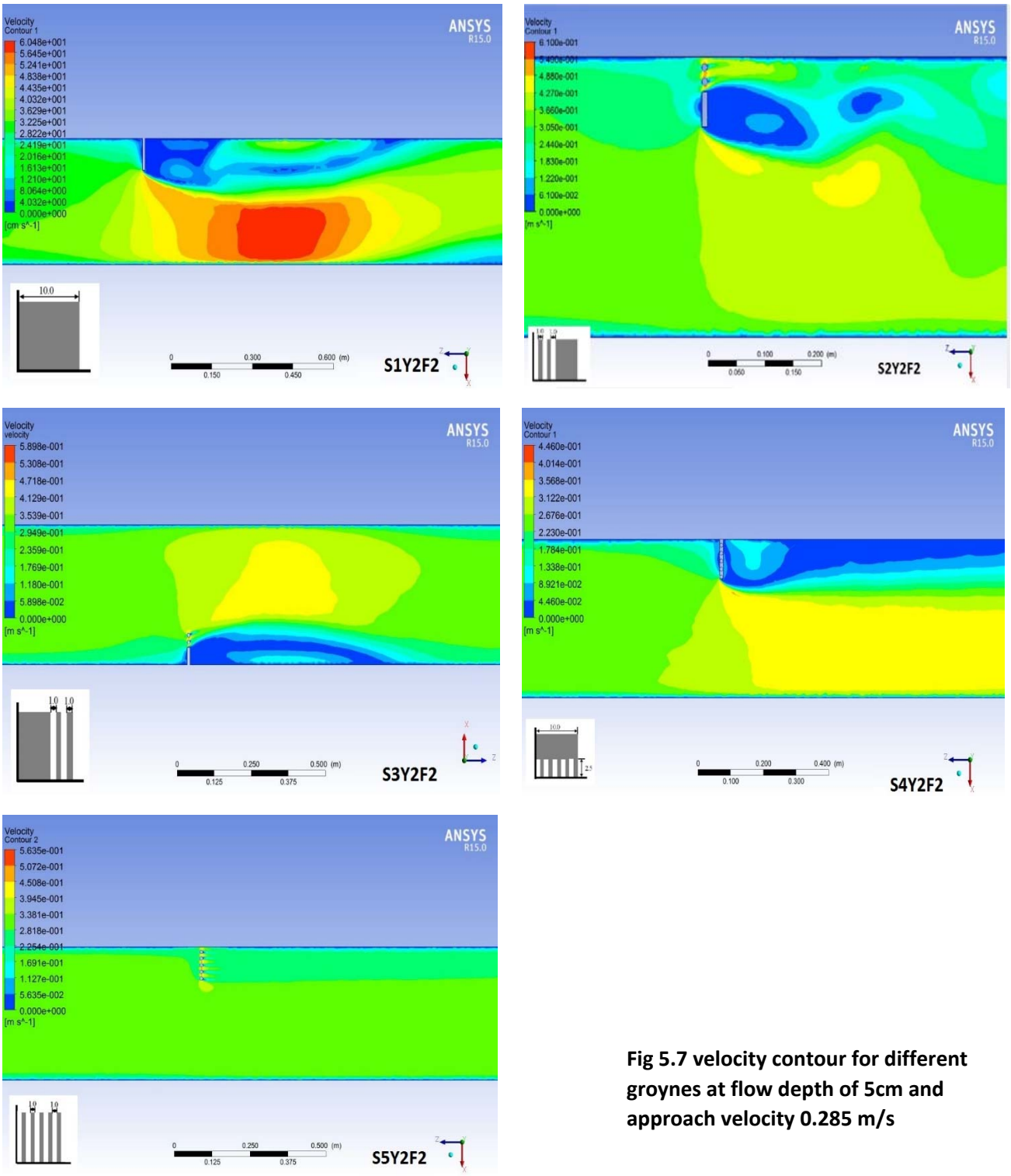

Fig 5.7 velocity contour for different groynes at flow depth of 5cm and approach velocity 0.285 m/s

5.8.2 Bed Shear Stress

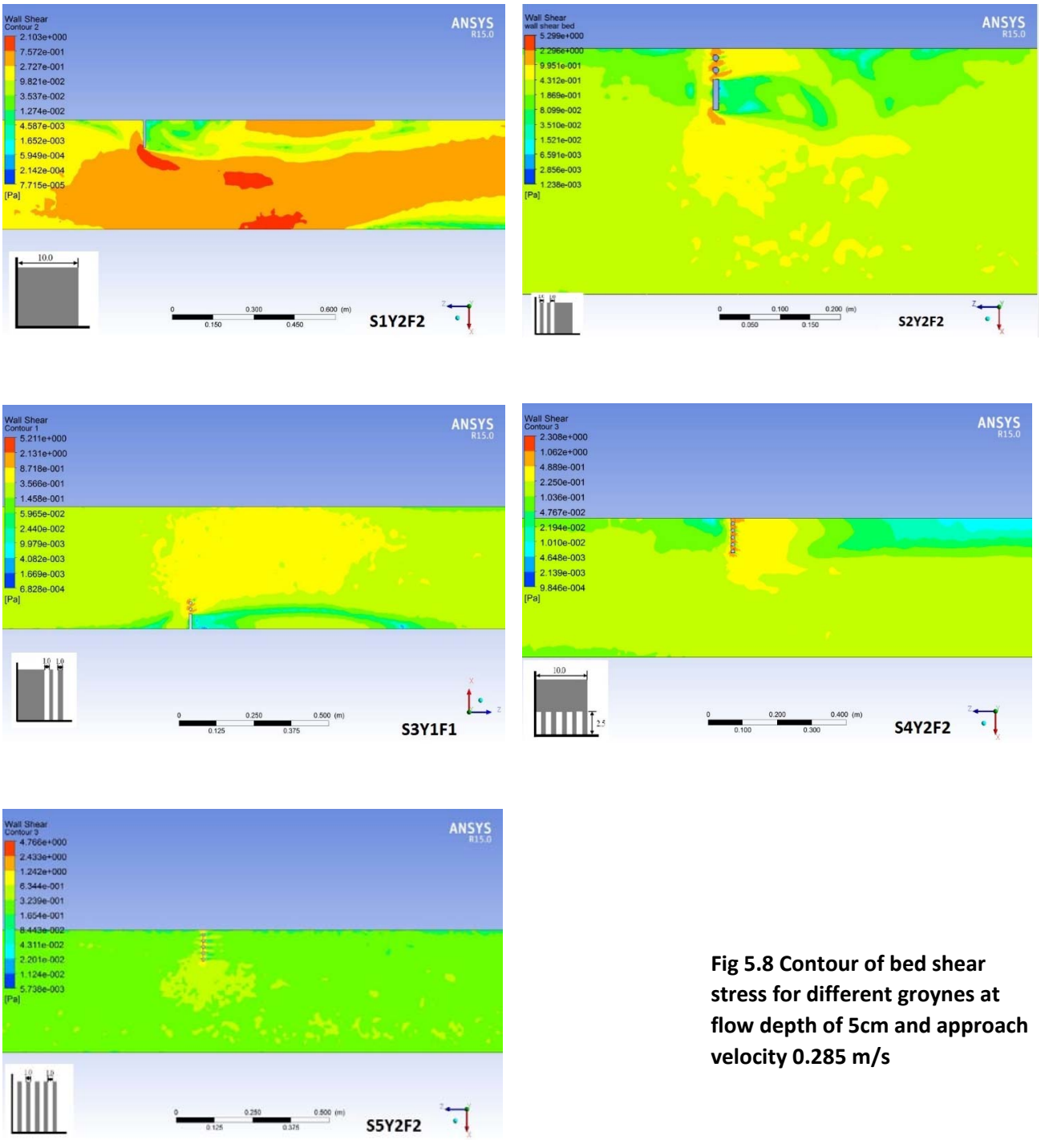

Fig 5.8 Contour of bed shear stress for different groynes at flow depth of 5cm and approach velocity 0.285 m/s

5.8.3 Velocity streamlines.

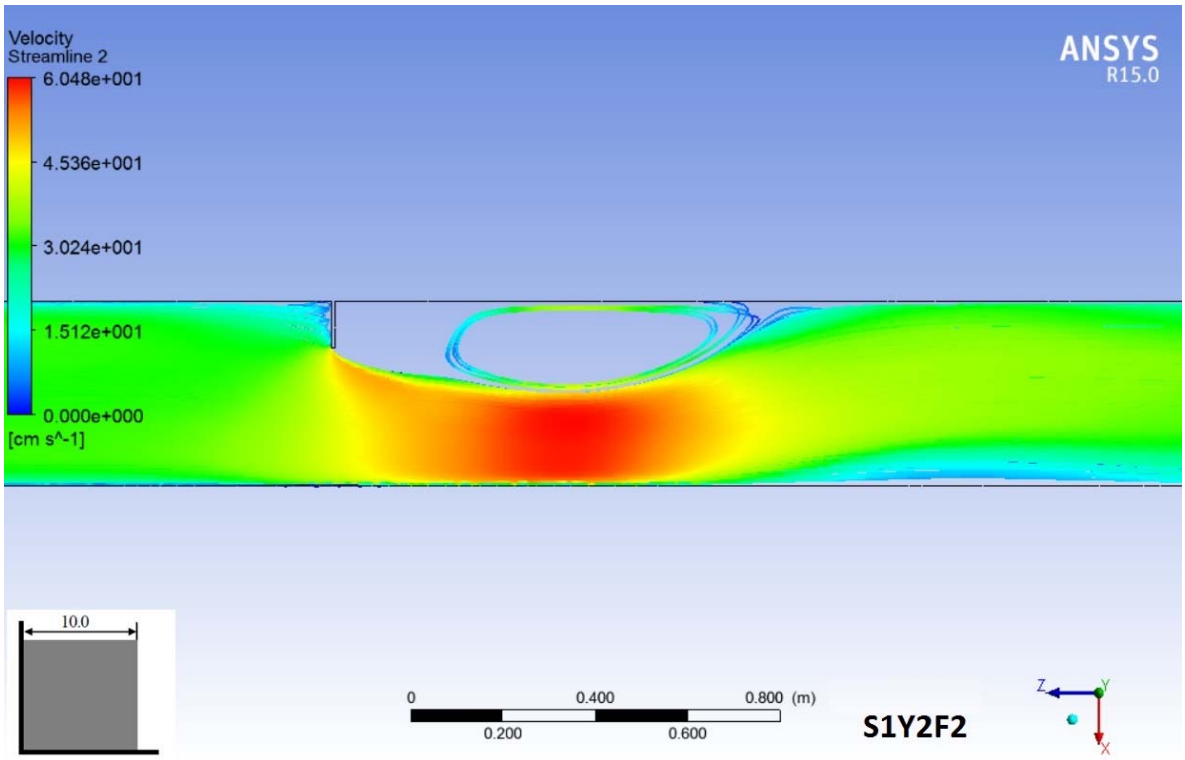

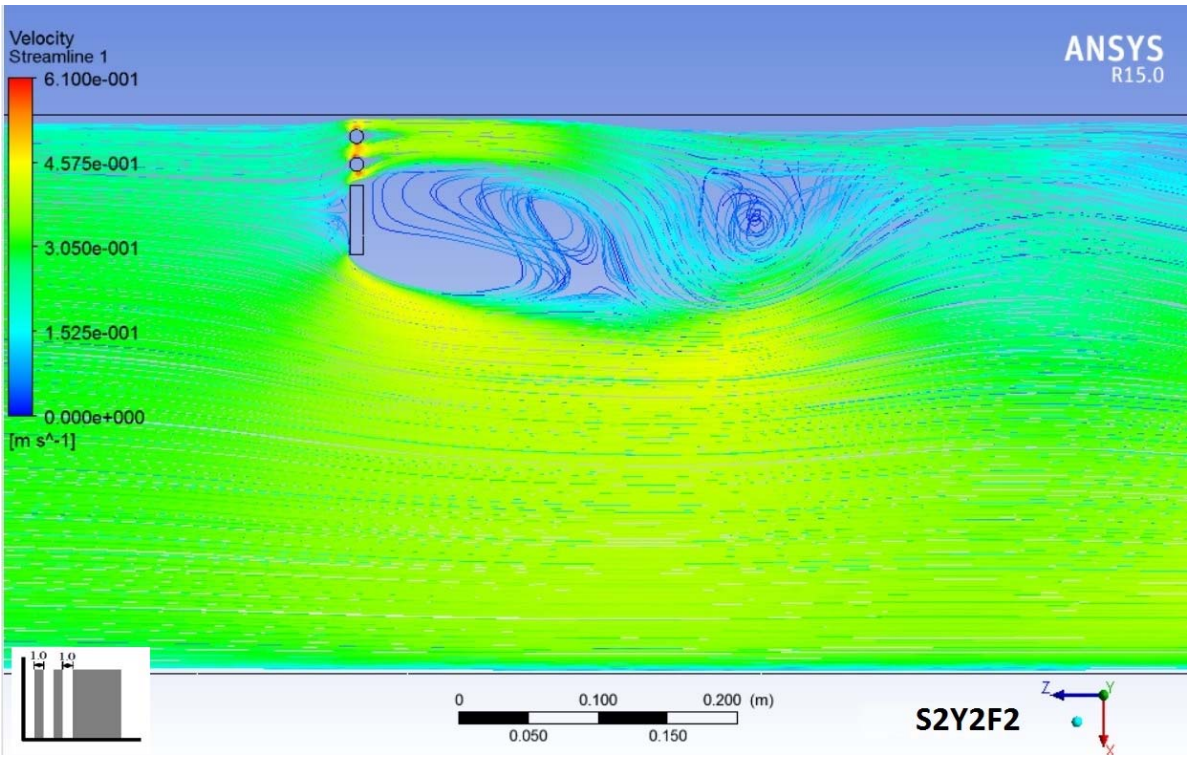

Fig 5.9 Stream lines for S1 and S2 spurs at flow depth of 5cm and approach velocity 0.285 m/s.

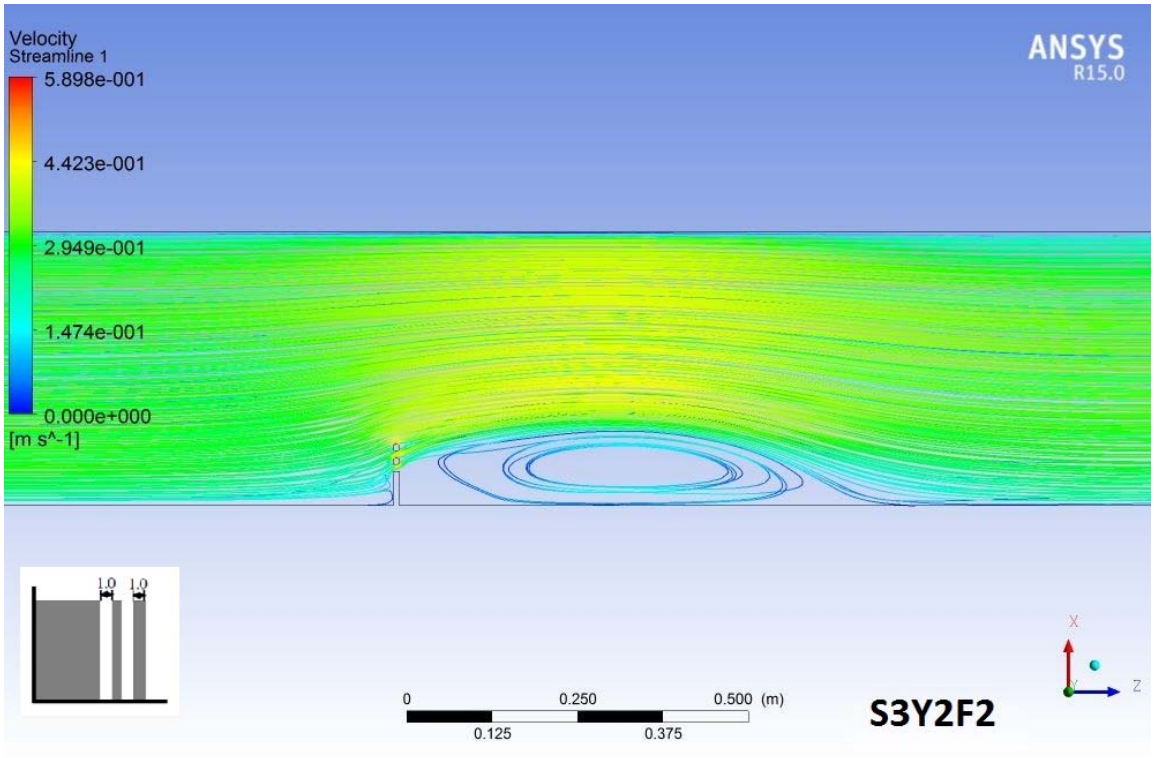

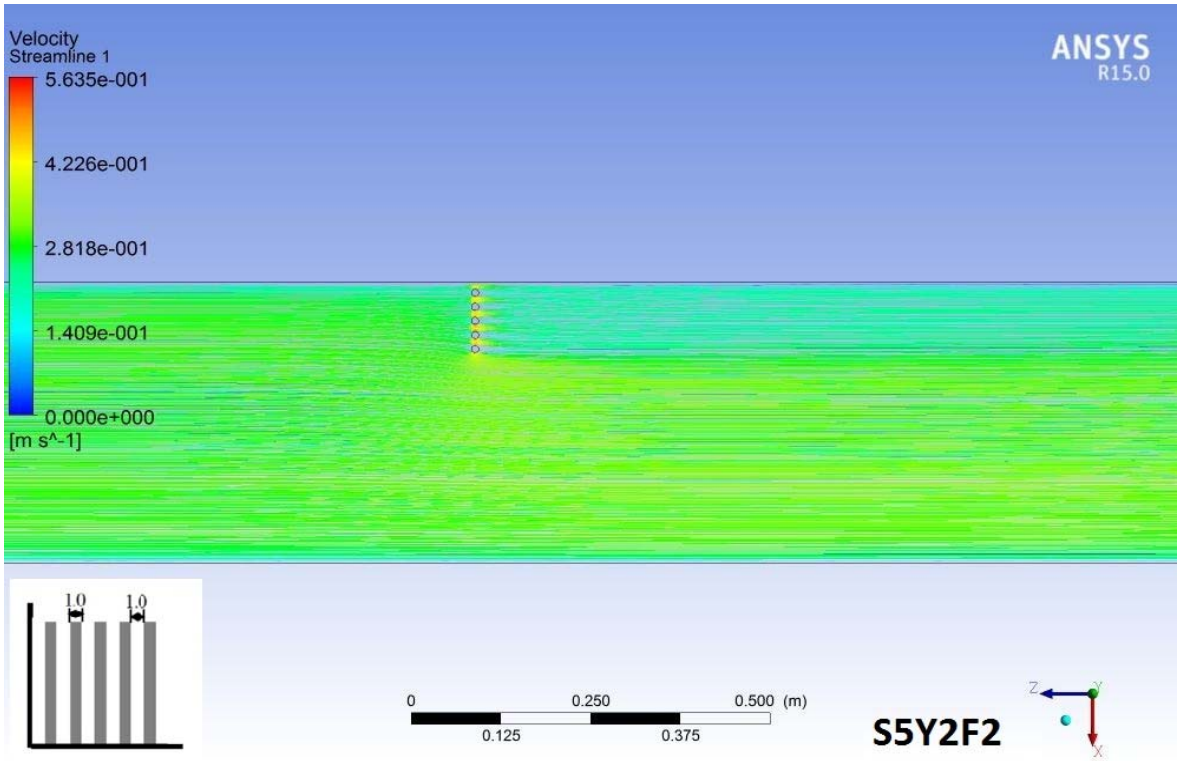

Fig 5.10 Stream lines for S3 and S5 spurs at flow depth of 5cm and approach velocity 0.285 m/s.

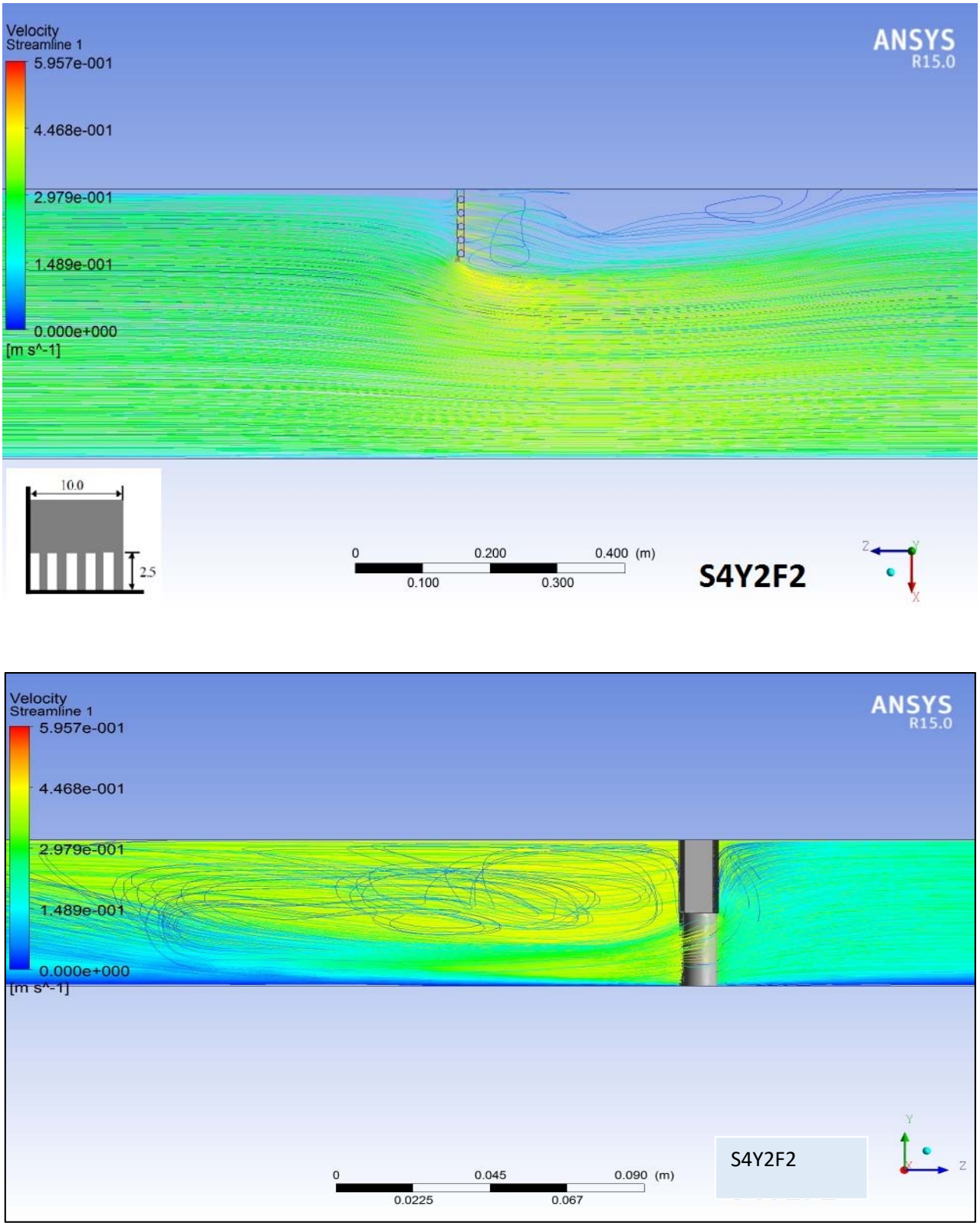

Fig 5.11 Streamlines for S4 at flow depth of 5cm and approach velocity 0.285 m/s

The velocity stream lines given above shows the characteristics of flow near spurs. A large vortex can be seen in case of impermeable spur. In case of spur 2 ie. Spur with permeable root two major vortices can be seen easily. Also it can be seen that the major vortex is separated from bank. The flow characteristics of third spur

S3 ie. The one with permeable tip shows little difference from spur of type 1 with smaller vortex region for spur3. In case of Spur 4 the top does not show much details of the complex flow involved. But views from other angles show that the vortices are formed in the upper flow region. The vortex is weak and is confined in the shade of the impermeable part of the structure and their effect on bed is minimized by the flow from permeable region resulting in reduced values of bed shear stress. In case of permeable spur 5 no major vortices are seen as the flow passes through the permeable region and with less disturbance.

CHAPTER 6-CONCLUSIONS

1) The realizable K-e model is validated for flow around spur dyke and percentage error in computing is found to be less than 10 %.
2) The tip velocity is found to increase upto a maximum of 1.54 times the approach velocity in case of impermeable spur dyke to a lowest of 1.16 times for permeable spur. Hybrid structures do show some drop in tip velocity owing to their permeability.
3) The tip velocity for hybrid spurs show lower values than impermeable spur. With spur3 and spur 4 showing considerable drop in tip velocity. Spur 4 shows lower maximum velocity than other hybrid and impermeable spur.
4) Impermeable spur shows maximum separation length of 13.2 times the spur length. Among other spurs considered spur4 ie bandall spur shows highest values for separation length of 7.5 to 8.5 times spur length.
5) Hybrid structures show lower bed shear amplification with spur 4 giving best results among hybrid spurs. Spur 4 shows bed shear values of about 1.5 times lower than that of impermeable spur. Spur 2 shows increased values of bed shear in some cases.
6) Based on the parameter of separation length and bed shear stress amplification results it is seen that bandall structure shows similar performance to that of impermeable groyne.
7) Streamlines of flow show a large vortex in the downstream of impermeable spur. And two major vortices in case of spur2. The streamlines for spur4 shows that vortices are formed in upper flow regions their strength is low towards bed. The flow from lower permeable part intercepts the vortices resulting in lower bed shear stress in case of spur 4 ie. Bandall structure.
8) From the plots of ratio of separation length and velocity amplification it can be seen that impermeable groyne provides best separation length, Bandall structure shows better results for separation length when compared with other hybrid structures and shows values comparable to impermeable groyne.

Overall Conclusion

9) On the basis of above conclusion it can be concluded that spur4 ie bandall like structure may be used as an alternative to impermeable groyne to achieve desired performance in terms of separation length with decreased bed shear stress values. the reduction in bed shear will result in reduced local scouring as compared to impermeable groyne. Also models can be developed to keep the bed shear stress under threshold shear stress.

Future scope of study

Study of hybrid groynes needs more study to understand the flow characteristics around these structures especially the bandall structure. In future studies these groynes can be tested for performance when installed in series. Other hybrid structures can also be purposed Also studies on moveable bed can be conducted. The study of behaviour of these groynes in case of surge pass is also needed.

References

1. Francis, J. R. D., A. B. Pattanaik, and S. H. Wearne. "Technical note.. Observations of flow patterns around some simplified groyne structures in channels." *ICE Proceedings*. Vol. 41. No. 4. Thomas Telford, 1968.
2. Rajaratnam, Nallamuthu, and Benjamin A. Nwachukwu. "Flow near groin-like structures." *Journal of Hydraulic Engineering* 109.3 (1983): 463-480.
3. Asayama, Chiharu."Study on Control for Suitable Bed Morphology around Successive Groynes".
4. Tingsanchali, Tawatchai, and Selvaratnam Maheswaran. "2-D depth-averaged flow computation near groyne." *Journal of Hydraulic Engineering* 116.1 (1990): 71-86.
5. Ouillon, Sylvain, and Denis Dartus. "Three-dimensional computation of flow around groyne." *Journal of hydraulic Engineering* 123.11 (1997): 962-970.
6. Mioduszewski, Tomasz, Shiro Maeno, and Yatsugi Uema. "Influence of the spur dike permeability on flow and scouring during a surge pass." *International Conference on Estuaries and Coasts*. 2003.
7. Ettema, Robert, and Marian Muste. "Scale effects in flume experiments on flow around a spur dike in flatbed channel." *Journal of Hydraulic Engineering* (2004).
8. Baba, Y., et al. "Flows and bedload dynamics around spur dyke in a compound channel." *11th International Symposium on River Sedimentation (ISRS)*. 2010
9. Uijttewaal, Wim S. "Effects of groyne layout on the flow in groyne fields: Laboratory experiments." *Journal of Hydraulic Engineering* (2005).
10. Yeo, Hong Koo, Joon Gu Kang, and Sung Jung Kim. "An experimental study on tip velocity and downstream recirculation zone of single groynes of permeability change." *KSCE Journal of Civil Engineering* 9.1 (2005): 29-38.
11. Kang, Joongu, et al. "Experimental investigation on the local scour characteristics around groynes using a hydraulic model." *Water and Environment Journal* 25.2 (2011): 181-191
12. Ghani, Usman, Shahid Ali, and Sabhat Arif. "Influence of Spur Dike on Flow Patterns in an Open Channel."
13. Ghaldarbandi.R., M. H. Keshavarz, and H. Hakimzadeh. "Investigation of the Bed and Structural Slopes on Bed Shear Stress and Flow Characteristics around an Impermeable Groyne." *Journal of Hydraulic Structures* 1.1 (2013): 11-23
14. Zhang, Hao, et al. "Experiment Study on Channel Bed Characteristics around Spur Dykes of Different Shapes." *Journal of Japan Society of Civil Engineers, Ser. A2 (Applied Mechanics (AM))* 69.2 (2013): I_489-I_499.
15. Yossef, Mohamed FM, and Huib J. de Vriend. "Flow details near river groynes: experimental investigation." *Journal of Hydraulic Engineering* 137.5 (2010): 504-516.
16. Tang, Xuelin, Xiang Ding, and Zhicong Chen. "Large eddy simulations of three-dimensional flows around a spur dike." *Tsinghua Science & Technology* 11.1 (2006): 117-123.
17. McCoy, Andrew, George Constantinescu, and Larry J. Weber. "Numerical investigation of flow hydrodynamics in a channel with a series of groynes."*Journal of Hydraulic Engineering* 134.2 (2008): 157-172.

18. Safarzadeh, A., et al. "Experimental study of head shape effects on shear stress distribution around a single groyne." *River flow 2010, Proceedings of 5th International Conference on Fluvial Hydraulics*. 2010.

19. Yazdi, J., et al. "3D simulation of flow around a single spur dike with free-surface flow." *Intl. J. River Basin Management* 8.1 (2010): 55-62.

20. Shahrokhi, Mahdi, and Hamed Sarveram. "Three-dimensional simulation of flow around a groyne with large-eddy turbulence model." *Journal of Food, Agriculture & Environment* 9.3&4 (2011): 677-681.

21. Hakimzadeh, H., Azari, N. and Mehrzad, R. "Experimental Study of the Effect of Lateral Structural Slopes of Groynes on Scour Reduction", Proceedings of Sixth International Conference on Scour and Erosion, Paris, France, 2012.

22. Mansoori, Amir-Reza, et al. "Three-Dimensional Features of the Turbulent Flow around Series of Groynes with Different Shapes of Head." *Journal of Japan Society of Civil Engineers, Ser. B1 (Hydraulic Engineering)* 68.4 (2012): I_61-I_66.

23. Acharya, Anu, and Jennifer G. Duan. "Three dimensional simulation of flow field around series of spur dikes." *ASCE copyright Proceedings of the 2011 World Environmental and Water Resources Congress, California, USA*. 2011.

24. Ghaldarbandi.R., M. H. Keshavarz, and H. Hakimzadeh. "Investigation of the Bed and Structural Slopes on Bed Shear Stress and Flow Characteristics around an Impermeable Groyne." *Journal of Hydraulic Structures* 1.1 (2013): 11-23

25. Shamloo, Hamid, and Bahareh Pirzadeh. "Numerical Simulation of the Angle of Groyne Installation on the Separation Zone Length Behind it." *Journal of River Engineering* 2 (2014).

26. Karami, Hojat, et al. "Verification of numerical study of scour around spur dikes using experimental data." *Water and Environment Journal* 28.1 (2014): 124-134.